ANALYSIS OF NON-NEWTONIAN POWER-LAW FLUIDS FLOW OVER A ROTATING BODY

Alexander Joseph Esseniyi

Submitted in Partial Fulfillment of the Requirement

for the Degree of

Master of Science in Engineering

in the

Mechanical Engineering Department

June 3, 1991

Adviser Date

Sally M. Hotchkiss June 4, 1991

Dean of the Graduate School Date

Youngstown State University

June 1991

To Kathleen

and Benjamin

ACKNOWLEDGEMENTS

With sincere gratitude I thank Dr. H. W. Kim for instructing me in my graduate course work on heat and fluid flow, and for being my thesis advisor. Dr. Kim's encouragement and guidance led me through times when I may have abandoned my goal. I will always admire and appreciate his knowledge and sharing of it with me.

I thank Drs. F. A. D'Isa, B. J. Kitchen, and G. Kudav for serving on my committee. Their time spent reviewing the manuscript and their constructive comments were greatly appreciated.

Gratitude is also extended to Commercial Intertech's Hydraulic Pump Division Engineering Department for use of the personal computer equipment to generate data and the manuscript, and for the time to meet with my advisor.

Finally, my wife and son, to whom this is dedicated, receive my greatest gratitude. For without their love, encouragement, and boundless patience I would have never completed this endeavor.

TABLE OF CONTENTS

LIST OF TABLES

LIST OF FIGURES

NOMENCLATURE

b_i - geometry coefficient

c_i - geometry coefficient

C_f - friction coefficient, defined by (4.2)

d_i - flow coefficient

f - dimensionless stream function, defined in (2.8a)

g - dimensionless tangential velocity, defined in (2.8b)

h - integrating step size, $\Delta\eta$

k_i - constant in Runge-Kutta formula, ref. (3.11)

K - consistency index for non-Newtonian viscosity

L - characteristic length

M_l - dummy variable, l=x or y

n - power-law exponent

r - distance from the axis of symmetry to a surface element

R - characteristic radius

Re - generalized Reynolds Number, defined by $(\rho/K)(L^n)(U_\infty)^{2-n}$

u - velocity component in x direction

U_e - velocity at the outer edge of the boundary layer

U_∞ - velocity of the incoming fluid, free stream velocity

v - velocity component in y direction

w - tangential velocity in direction of rotation

W - rotation parameter, defined by $L\Omega/U_\infty$

x - coordinate measured along surface from forward stagnation point

x_j - abscissa in Runge-Kutta formula, ref. (3.11)

y - coordinate normal to surface

y_j - ordinate in Runge-Kutta formula, ref.(3.11)

z - coordinate perpendicular to x and y, defined by 'Right-Hand' rule

η - transformed dimensionless coordinate, defined by (2.7b)

Λ - wedge parameter, defined by (2.14)

μ - fluid viscosity defined by Newton Law of Friction

μ_{app} - apparent fluid viscosity, defined by (1.1)

ξ - transformed dimensionless coordinate, defined by (2.7a)

ρ - fluid density

τ_{xy} - shear stress, defined by (2.5a)

τ_{zy} - shear stress, defined by (2.5b)

τ_w - wall shear stress, defined by (4.1)

ψ - transformed dimensionless variable, defined by (2.7c)

ω - angular velocity, defined by (2.4a)

Ω - angular velocity of the axisymmetric body

An Abstract of

ANALYSIS OF NON-NEWTONIAN POWER-LAW FLUIDS

FLOW OVER A ROTATING BODY

Alexander Joseph Esseniyi

Submitted in Partial Fulfillment of the Requirement
for the Degree of
Master of Science in Engineering
in the
Mechanical Engineering Department
Youngstown State University
June 1991

The present analysis considers the momentum transfer within a laminar boundary layer of non-Newtonian power-law fluids flow over a rotating axisymmetrical body. The work is an extension of a previous analysis of power-law fluid flow over a non-rotating axisymmetrical body. Newtonian fluids, as well, are evaluated within the scope of this paper.

A generalized coordinate transformation is utilized with a Merk-Meksyn series expansion to transform the nonlinear governing momentum equations into a set of coupled ordinary differential equations. The first three terms of the set are derived for general evaluation. The first term equations are numerically integrated for a non-rotating and rotating sphere to obtain the axial and tangential velocity gradients. The Runge-Kutta method for numerical integration is used with the control of integrating step size. The iteration procedure is the Newton-Raphson technique. The friction coefficient is then determined using the velocity gradients and presented in the form of $1/2C_fRe^{1/(n+1)}$.

The initial velocity gradients and friction coefficients for Newtonian fluids are tabulated and compared to the results from Lee, Jeng, and DeWitt for equivalent values of n. Likewise, the initial axial velocity for non-rotating bodies is compared to the results of Kim. The non-Newtonian portion of this analysis compares the friction coefficient for three values of n to the published results of Kleinstreuer and Wang. Axial and tangential velocities through the boundary layer for Newtonian and non-Newtonian fluids are also graphically shown.

Chapter I. Introduction

1.1 Classification of Fluids

Fluid dynamics theory has developed from the early stages of studying 'Ideal' fluids or fluid that is incompressible and void of viscosity or elasticity, to studying and developing models of 'Real' fluids. These real fluids are divided into two large generic classes depending on the relationship of shear stress and strain rate at a constant temperature. The most commonly studied fluid is Newtonian, which exhibits a linear relationship between shear stress and strain rate, and includes all gases and liquids or solutions of low molecular weight materials. Fluids which have a non-linear, shear-stress, strain-rate relationship are collectively considered non-Newtonian, and are further subdivided into three broad categories: time-independent fluids, time-dependent fluids, and viscoelastic fluids. In reality, however, no fluid can be distinctly defined into any one of these categories.

The largest grouping of non-Newtonian fluids is encompassed within the time-independent classification, which can be further broken down into fluids that exhibit a yield stress and fluids that do not. The Power-Law, or Ostwald de Waele, model predominates studies of no-yield-stress fluids due to the linear logarithmic relationship that exists between the shear stress and strain rate for the materials. The model also readily includes Newtonian fluids and is expressed as $\tau_{xy} = K(\partial u/\partial y)^n$. The "consistency index" [1] K, can only be defined as dynamic viscosity when n is unity. The comparison of the Power-Law model with the Newtonian model, $\tau = \mu(du/dy)$, has led many authors to define an *apparent viscosity* as;

$$\mu_{app} = \frac{\tau}{\frac{\partial u}{\partial y}} \qquad or, \qquad \mu_{app} = \frac{K}{\left(\frac{\partial u}{\partial y}\right)^{1-n}} \tag{1.1a,b}$$

with $\tau = \tau_{xy}$. The value of μ_{app} is essentially meaningless for non-Newtonian fluids unless it is associated with a reference shear stress or strain rate. The value of the power index, n, serves to divide Power-Law fluids further into Pseudo-plastic fluids for n less than unity, and Dilatant fluids for n greater than unity.

Pseudo-plastics comprise the majority of non-Newtonian fluids found in typical applications, and with $n<1$ show an apparent viscosity that decreases with an increasing strain rate. Examples of pseudo-plastic materials are: rubber solutions, adhesives, polymer solutions or melts, greases, mayonnaise, soap, paper pulp, paints, and biological fluids.

Dilatant fluids are far less common than pseudo-plastics and show the opposite rheological characteristic of increasing apparent viscosity with an increasing strain rate. The following materials exemplify dilatant behavior: some aqueous suspensions of titanium dioxide, some corn flour/sugar solutions, potassium silicate, quicksand, iron powder in low-viscosity liquids, and wet beach sand.

1.2 Momentum Transfer of Power-Law Fluids

The definition of flow characteristics created by rotating axisymmetric bodies placed in a forced uniform flow stream is important for the analysis of problems involving rotary machine design, ballistics, re-entry vehicles, and fiber coating applications. While the majority of applications, especially in industry, apply to Newtonian fluids there is a large area of interest in non-Newtonian fluids such as molten plastics, pulp, food stuffs, slurries, biological fluids, and emulsions. The difficulty in analyzing power-law flows, due to the nonlinearity of the shear stress term in the governing equations, is complicated by the addition of the tangential velocity of the rotating body.

One of the first, if not *the first*, analyses made of non-Newtonian fluids in laminar boundary layer flow over a body was done by Acrivos, Shah, and Petersen [2]. Their paper dealt with predicting the drag and rate of heat transfer from an isothermal surface to the fluid. A similarity solution was utilized to solve the momentum equation for a flat plate and determine the drag coefficient. Since then repeated use of similarity solutions has been extensive for momentum equations. Attempts were made to use the integral method of solution which was initiated by Pohlhausen with respect to Newtonian flows. It however showed poor accuracy in predicting the drag coefficient when compared to analytic solutions, and therefore is not applicable for use in conjunction with energy transfer solutions - the end-use purpose for momentum solutions.

Lee and Ames [3] extensively explored the use of similarity solutions for power-law fluids to determine: momentum transfer in general Falkner-Skan flows and Goldstein flows; momentum and energy transfer in forced convection about a right angle wedge; natural convection with constant heat flux at the boundary surface; and general Falkner-Skan flows with nonconstant heat conductivity and restricted surface temperature distribution. They also applied similarity transformations for momentum and heat transfer of Eyring viscous fluids about a right angle wedge.

Merk [4] utilized Meksyn's "Wedge Method" of transformation to determine a new technique to analyze laminar boundary layer flow. This transformation allowed Merk to reduce the governing equations from nonlinear partial differential equations to ordinary differential equations. The equations were defined using universal functions eliminating dependence on actual body geometry. The method has been compared with similarity transformation techniques and experimental data, and found to be fairly accurate. Chao and Fagbenle [5], presented a refined Merk-Meksyn methodology after finding errors with the second term in Merk's expansion. Chao's refined version of the Merk-Meksyn method has been applied to non-rotating-body Newtonian flows as in the Kim and Jeng [6] analysis of near separating flow; and to rotating body analyses by Jeng, DeWitt, and Lee [7], and Lee, Jeng, and DeWitt [8].

Analysis of power-law flow over stationary bodies has been studied more frequently in recent years. Kim [9] examined power-law flow over non-rotating axisymmetrical bodies for momentum and heat transfer characteristics. He later expanded his work in Kim, Jeng, and DeWitt [10] to include non-isothermal bodies. Kleinstreuer and Wang [11] have recently evaluated mixed thermal convection of power-law fluids past standard bodies with suction or injection, and axisymmetric body rotation. A coordinate transformation was used to reduce the original governing equations, then an implicit finite difference technique was employed to solve the resultant governing equations.

The present analysis studies the momentum transfer of laminar boundary layer power-law fluid flow past a rotating axisymmetric body. The work is an extension of the previously cited non-rotating analysis by Kim [9]. It utilizes a coordinate transformation along with the Merk-Meksyn series expansion, as refined by Chao et al. [5], as it studies the first term of the expansion. The first term axial and tangential velocities, friction coefficient values, and velocity profiles are presented.

Chapter II. Formulation of Governing Equations

2.1 General Assumptions and Description of Problem

The following assumptions were applied to this momentum boundary layer analysis for power-law fluids:

i) Fluid compressibility is negligible, i.e. incompressible fluid.

ii) All physical quantities, such as density, are constant.

iii) The boundary layer that develops over an axisymmetrical body within a uniform stream is laminar.

iv) The stream flow beyond the boundary layer is considered as potential flow.

v) External body forces are negligible.

vi) The angular velocity of the axisymmetrical body is constant.

The coordinate system is defined such that the x coordinate is measured from the forward stagnation point along the surface defined by a plane cutting through the axis of symmetry of the body. The y coordinate is the outer normal to the body contained in the plane, and the z coordinate is defined by the use of the 'right-hand' rule. The distance from the axis of symmetry to a surface element is defined as 'r', which for an axisymmetrical body is a function of x only. The velocities u, v, and w correspond directionally with the x, y, and z coordinates respectively. The body is rotating at a constant angular velocity with its axis parallel to the direction of the free stream. The above problem is depicted in Fig. 2.1.

2.2 Governing Boundary Layer Equations

The general boundary layer equations are as follows for the above stated conditions:

<u>Continuity Equation</u>

$$\frac{\partial(ru)}{\partial x} + \frac{\partial(rv)}{\partial y} = 0 \tag{2.1}$$

<u>Momentum Equations</u>

$$u\frac{\partial u}{\partial x} + v\frac{\partial u}{\partial y} - \frac{w^2}{r}\frac{dr}{dx} = U_e\frac{dU_e}{dx} + \frac{1}{\rho}\frac{\partial(\tau_{xy})}{\partial y} \tag{2.2}$$

$$u\frac{\partial w}{\partial x} + v\frac{\partial w}{\partial y} + \frac{uw}{r}\frac{dr}{dx} = \frac{1}{\rho}\frac{\partial(\tau_{zy})}{\partial y} \tag{2.3}$$

with the boundary conditions:

$$@y=0 \qquad u=v=0, \qquad w=r\omega \tag{2.4a}$$

$$\text{as } y\to\infty \qquad u=U_e(x), \qquad v=w=0 \tag{2.4b}$$

where $U_e(x)$ is the main stream velocity just outside the boundary layer. The shear stresses can be defined for the power-law fluids, using Equation (1.1), as;

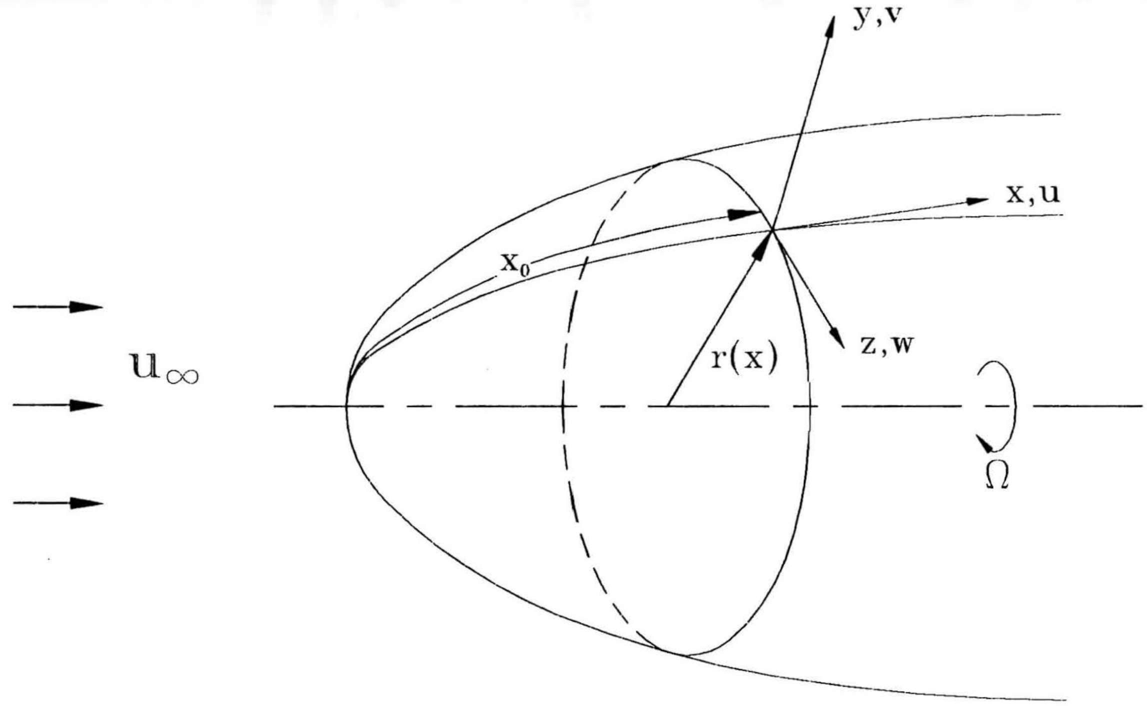

Fig. 2–1 Physical Model And The Coordinate System

$$\tau_{xy} = K\left|\frac{\partial u}{\partial y}\right|^{n-1}\frac{\partial u}{\partial y}\ , \qquad \tau_{zy} = K\left|\frac{\partial w}{\partial y}\right|^{n-1}\frac{\partial w}{\partial y} \tag{2.5a,b}$$

where n and K are constants. The dimensionless fluid index parameter is n, and K can dimensionally be expressed in lbf-$\text{sec}^n\text{-ft}^2$. The above Governing Equations can be adapted for use with two-dimensional bodies by replacing r with L, a reference length.

2.3 Coordinate Transformation

A stream function, $\psi(x,y)$, is introduced to satisfy the continuity equation such that

$$u = \frac{1}{r}\frac{\partial\psi}{\partial y}\ , \qquad v = -\frac{1}{r}\frac{\partial\psi}{\partial x} \tag{2.6a,b}$$

The (x,y) coordinate system is transformed into a dimensionless system by utilizing the following dimensionless variables;

$$\xi = \frac{n}{L}\int_0^x\left(\frac{r}{L}\right)^{n+1}\left(\frac{U_e}{U_\infty}\right)^{2n-1}dx \tag{2.7a}$$

$$\eta = \left[\frac{Re}{(n+1)\,\xi}\right]^{\frac{1}{n+1}}\left(\frac{U_e}{U_\infty}\right)\left(\frac{r}{L}\right)\frac{y}{L} \tag{2.7b}$$

where Re is a generalized Reynolds Number and $Re=(\rho/K)(L^n)(U_\infty)^{2-n}$. The stream function and w are now defined as;

$$\psi = \left[\frac{(n+1)\xi}{Re}\right]^{\frac{1}{n+1}} (U_\infty L^2)\, f(\xi,\eta) \tag{2.8a}$$

$$w = r\Omega\, g(\xi,\eta) \tag{2.8b}$$

where f is a dimensionless stream function, and g is a dimensionless tangential velocity perpendicular to the (x,y) coordinates. Equations (2.6a,b) become

$$u = U_e \frac{\partial f}{\partial \eta} \tag{2.9}$$

$$v = -\frac{nU_\infty L}{r}\left(\frac{r}{L}\right)^{n+1}\left(\frac{U_e}{U_\infty}\right)^{2n-1}(Re)^{-\frac{1}{n+1}}[(n+1)\xi]^{-\frac{n}{n+1}}$$
$$\left[f + (n+1)\xi\frac{\partial f}{\partial \xi} + \left[\Lambda + \frac{(n+1)\xi dr}{r d\xi} - 1\right]\eta\frac{\partial f}{\partial \eta}\right] \tag{2.10}$$

respectively. Utilizing Equations (2.5), (2.9), and (2.10), the momentum Equations (2.2) and (2.3) become,

$$(|f''|^{n-1} f'')' + nff'' + n\Lambda[1-(f')^2] +$$
$$\frac{n(n+1)\xi}{r}\frac{dr}{d\xi}\left(\frac{r\Omega}{U_e}\right)^2 g^2 = n(n+1)\xi\frac{\partial(f',f)}{\partial(\xi,\eta)} \tag{2.11}$$

$$(|g'|^{n-1}g')' + n\left(\frac{r\Omega}{U_e}\right)^{1-n} fg' -$$
$$\frac{2n(n+1)\xi}{r}\frac{dr}{d\xi}\left(\frac{\Omega r}{U_e}\right)^{1-n} f'g = n(n+1)\xi\left(\frac{\Omega r}{U_e}\right)^{1-n}\left(\frac{\partial(g,f)}{\partial(\xi,\eta)}\right) \tag{2.12}$$

where the prime denotes differentiation with respect to η and the Jacobians in Equations (2.11) and (2.12) are,

$$\frac{\partial(f',f)}{\partial(\xi,\eta)} = \frac{\partial f'}{\partial \xi}f' - f''\frac{\partial f}{\partial \xi} \tag{2.13a}$$

$$\frac{\partial(g,f)}{\partial(\xi,\eta)} = \frac{\partial g}{\partial \xi} f' - g' \frac{\partial f}{\partial \xi} \tag{2.13b}$$

The parameter Λ, in Equation (2.11), is referred to as the 'wedge variable' by Merk and is solely a function of ξ, i.e. x only. The following is the definition of Λ, which shows if U_e is known, then Λ can be explicitly determined.

$$\Lambda = \frac{(n+1)\xi}{U_e} \frac{L}{n} \left(\frac{r}{L}\right)^{-n-1} \left(\frac{U_e}{U_\infty}\right)^{1-2n} \frac{dU_e}{dx} \tag{2.14}$$

The boundary conditions for Equations (2.11) and (2.12) are,

$$@\eta = 0 \qquad f(\xi,0) = f'(\xi,0) = 0 \qquad g(\xi,0) = 1 \tag{2.15a}$$

$$@\eta = \infty \qquad f'(\xi,\infty) \to 1 \qquad g(\xi,\infty) \to 0 \tag{2.15b}$$

Since there exists a one-to-one correspondence between Λ and ξ (or x) the Merk-Meksyn series expansion technique can be employed to redefine $f(\xi,\eta,n)$ and $g(\xi,\eta,n)$ as follows

$$f(\xi,\eta,n) = f_0(\Lambda,\eta,n) + (n+1)\xi \frac{d\Lambda}{d\xi} f_1(\Lambda,\eta,n) + (n+1)^2 \xi^2 \frac{d^2\Lambda}{d\xi^2} f_2(\Lambda,\eta,n) + \left[(n+1)\xi \frac{d\Lambda}{d\xi}\right]^2 f_3(\Lambda,\xi,n) + \cdots \tag{2.16a}$$

$$g(\xi,\eta,n) = g_0(\Lambda,\eta,n) + (n+1)\xi \frac{d\Lambda}{d\xi} g_1(\Lambda,\eta,n) + (n+1)^2 \xi^2 \frac{d^2\Lambda}{d\xi^2} g_2(\Lambda,\eta,n) + \left[(n+1)\xi \frac{d\Lambda}{d\xi}\right]^2 g_3(\Lambda,\eta,n) + \cdots \tag{2.16b}$$

Also the quantities

$$\frac{(n+1)\xi}{r} \frac{dr}{d\xi} \left(\frac{r\Omega}{U_e}\right)^2, \qquad \frac{2(n+1)\xi}{r} \frac{dr}{d\xi}, \qquad \left(\frac{r\Omega}{U_e}\right)^{1-n}$$

found in the Momentum Equations (2.11) and (2.12), are functions of x only. Therefore, they can be expressed in terms of Λ as follows:

$$\frac{(n+1)\xi}{r}\frac{dr}{d\xi}\left(\frac{r\Omega}{U_e}\right)^2 =$$

$$W^2\left[b_0\Lambda + (n+1)\xi\frac{d\Lambda}{d\xi}b_1 + (n+1)^2\xi^2\frac{d^2\Lambda}{d\xi^2}b_2 + (n+1)^2\xi^2\left(\frac{d\Lambda}{d\xi}\right)^2 b_3 + \cdots\right] \quad (2.17)$$

$$\frac{2(n+1)\xi}{r}\frac{dr}{d\xi} =$$

$$c_0\Lambda + (n+1)\xi\frac{d\Lambda}{d\xi}c_1 + (n+1)^2\xi^2\frac{d^2\Lambda}{d\xi^2}c_2 + (n+1)^2\xi^2\left(\frac{d\Lambda}{d\xi}\right)^2 c_3 + \cdots \quad (2.18)$$

$$\left(\frac{r\Omega}{U_e}\right)^{1-n} = W^{1-n}\left[d_0 + (n+1)\xi\frac{d\Lambda}{d\xi}d_1\right]^{1-n} +$$

$$W^{1-n}\left[(n+1)^2\xi^2\frac{d^2\Lambda}{d\xi^2}d_2 + (n+1)^2\xi^2\left(\frac{d\Lambda}{d\xi}\right)^2 d_3 + \cdots\right]^{1-n} \quad (2.19)$$

where W is the rotation parameter defined by $W=L\Omega/U_\infty$, and the coefficients b_i, c_i, and d_i are the constants for a particular combination of flow and body geometry.

Substituting Equations (2.16), (2.17), (2.18), and (2.19) into Equations (2.11) and (2.12) and subsequently arranging terms not containing $d\Lambda/d\xi$, and terms with $(n+1)\xi(d\Lambda/d\xi)$, $(n+1)^2\xi^2(d^2\Lambda/d\xi^2)$, $[(n+1)\xi(d\Lambda/d\xi)]^2$, $\cdots$ respectively, creates a set of coupled ordinary differential equations. The first set of equations becomes

$$f_0'''(|f_0''|^{n-2}f_0'') + f_0 f_0'' + \Lambda\left[1-(f_0')^2 + b_0 W^2 g_0^2\right] = 0 \quad (2.20a)$$

$$g_0''(|g_0'|^{n-2}g_0') + (d_0 W)^{1-n} f_0 g_0' - c_0 (d_0 W)^{1-n}\Lambda f_0' g_0 = 0 \quad (2.20b)$$

with boundary conditions:

$$f_0(0) = f_0'(0) = 0\,, \qquad g(0) = 1 \tag{2.20c}$$

$$f_0'(\infty) = 1\,, \qquad g_0(\infty) = 0 \tag{2.20d}$$

Collecting terms containing $(n+1)\xi(d\Lambda/d\xi)$ creates the second set of equations:

$$f_1'''(|f_0''|^{n-2} f_0'') + (n-1)|f_0''|^{n-2} f_1'' f_0''' + f_0 f_1'' + f_1 f_0'' - 2\Lambda f_0' f_1' + W^2(b_1 g_0^2 + 2b_0 \Lambda g_0 g_1) + (n+1)(f_1 f_0'' - f_1' f_0') = \frac{\partial(f', f)}{\partial(\Lambda, \eta)} \tag{2.21a}$$

$$g_1''(|g_0'|^{n-2} g_0') - (n-1) g_1' g_0'' |g_0'|^{n-2} + W^{1-n}\left[d_0^{1-n}(f_1 g_0' + f_0 g_1') + (n-1) d_0^{-n} d_1 f_0 g_0'\right] - W^{1-n} c_0 d_0^{1-n} \Lambda (f_0' g_1 + f_1' g_0) - W^{1-n} f_0' g_0 \left[c_1 d_0^{1-n} + (n-1) c_0 d_0^{-n} d_1 \Lambda\right] = W^{1-n} d_0^{1-n}\left[\frac{\partial(g_0, f_0)}{\partial(\Lambda, \eta)} + (n+1)(g_1 f_0' - f_1 g_0')\right] \tag{2.21b}$$

with boundary conditions:

$$f_1(0) = f_1'(0) = g_1(0) = 0 \tag{2.21c}$$

$$f_1'(\infty) = g_1(\infty) = 0 \tag{2.21d}$$

The third set of equations is obtained by collecting terms containing $(n+1)^2\xi^2(d^2\Lambda/d\xi^2)$:

$$f_2'''(|f_0''|^{n-2} f_0'') + (n+1)|f_0''|^{n-2} f_0''' f_2'' + f_0 f_2'' + 2(\Lambda - n - 1) f_0' f_2' + (2n-3) f_0'' f_2 + W^2(b_2 g_0^2 + 2b_0 \Lambda g_0 g_2) = f_1' f_0' - f_1' f_0'' \tag{2.22a}$$

$$
\begin{aligned}
&g_2''(|g_0'|^{n-2}g_0') - (n-1)|g_0'|^{n-2}g_0''g_2' + \\
&W^{1-n}\left[d_0^{1-n}(f_0g_2' + f_2g_0') + (n-1)\,d_0^{1-n}d_2f_0g_0'\right] - \\
&\quad W^{1-n}c_0d_0^{1-n}\Lambda(f_0'g_2 + f_2'g_0) - \\
&\quad W^{1-n}f_0'g_0\left[c_2d_0^{1-n} + (n-1)\,c_0d_0^{-n}d_2\Lambda\right] = \\
&\quad W^{1-n}d_0^{1-n}\left[g_1f_0' + 2(n+1)\,g_2f_0' - f_1g_0' - 2(n+1)\,f_2g_0'\right]
\end{aligned}
\tag{2.22b}
$$

with boundary conditions:

$$f_2(0) = f_2'(0) = g_2(0) = 0 \tag{2.22c}$$

$$f_2'(\infty) = g_2(\infty) = 0 \tag{2.22d}$$

The development of the above equations and later discussion of the perturbation equations required analysis of the *sign* of the functions f_o'' and g_o' and the partial derivatives of the *'apparent viscosity'* terms $|f_o''|$ and $|g_o'|$ with respect to x and y; $|f_o''|_x$, $|f_o''|_y$, $|g_o'|_x$, and $|g_o'|_y$. For the given physical model, it can be shown that the $|f_o''| = f_o''$, since f_o'' remains positive within the boundary layer. Likewise, $|g_o'| = -g_o'$ due to the fact that $1 \geq g_o \geq 0$ and the asymptotic nature of g_o causes g_o' to be negative within the boundary layer.

A computer program was developed for the numerical integration of the first set of equations, f_o and g_o, and is presented next.

Chapter III. Numerical Analysis of f_o and g_o Equations

Equation (2.20a),

$$f_0'''(|f_0''|^{n-2}f_0'') + f_0f_0'' + \Lambda\left[1 - (f_0')^2 + b_0W^2g_0^2\right] = 0$$

can be simplified into the following form:

$$f_0''' + f_0f_0''|f_0''|^{1-n} + \Lambda|f_0''|^{1-n}\left[1 - (f_0')^2 + b_0W^2g_0^2\right] = 0 \qquad (3.1)$$

which is nonlinear with respect to the power of n. It is also uncalculable at the edge of the boundary layer depending on the value of the parameter n, since the asymptotic boundary condition, $f''(\infty)$, must approach zero and unity minus the power-law index is negative for dilatant fluids.

Likewise, Equation (2.20b) can be written as,

$$g_0'' + (d_0W)^{1-n}|g_0'|^{1-n}\left[f_0g_0' - c_0\Lambda f_0'g_0\right] = 0 \qquad (3.2)$$

Again the equation suffers from difficulty at the edge of the boundary layer. Also, for dilatant fluids the equations actually become two-point boundary value problems leading to a finite value for η_∞, as pointed out by Acrivos, et al. [2].

The uncalculable condition at the outer edge of the boundary layer for f_0 in the second and third terms is addressed by applying L'Hospital's Rule to a rewritten Equation (3.1),

$$f_0''' = |f_0''|^{1-n}\left[-f_0 f_0'' - \Lambda\left(1 - (f_0')^2 + b_0 W^2 g_0^2\right)\right] \tag{3.3a}$$

or,

$$f_0''' = \frac{-f_0 f_0'' - \Lambda\left(1 - (f_0')^2 + b_0 W^2 g_0^2\right)}{|f_0''|^{n-1}} \tag{3.3b}$$

The $\lim_{\eta\to\infty}$ is applied to the RHS of Equation (3.3b), and the equation becomes:

$$(f_0''')^2 + \frac{f_0|f_0''|^{2-n}}{n-1}(f_0''') + \frac{|f_0''|^{2-n}}{n-1}\left[f_0' f_0'' - 2\Lambda\left(f_0' f_0'' - b_0 W^2 g_0 g_0'\right)\right] = 0 \quad as \ \eta\to\infty \tag{3.4}$$

The above quadratic equation is solved as;

$$f_0''' = -\frac{0.5}{n-1} f_0|f_0''|^{2-n} \pm \frac{0.5}{n-1}\sqrt{f_0^2|f_0''|^{4-2n} - 4|f_0''|^{2-n}(n-1)\left[f_0' f_0'' - 2\Lambda\left(f_0' f_0'' - b_0 W^2 g_0 g_0'\right)\right]} \tag{3.5}$$

The choice of the *sign (±)* for the square root function depends on the convergence of the solution. Previous work, i.e. Kim [9], has shown that the positive sign caused the solution to oscillate, therefore the negative sign is used.

Applying the same principles to the second term in Equation (3.2), yields;

$$g_0'' = \frac{-(d_0 W)^{1-n}\left[f_0 g_0' - c_0 \Lambda f_0' g_0\right]}{|g_0'|^{n-1}} \tag{3.6}$$

Now applying $\lim_{\eta\to\infty}$ to the RHS of the equation and simplifying, Equation (3.6) becomes;

$$(g_0'')^2 + \frac{(d_0 W)^{1-n} f_0 |g_0'|^{2-n}}{n-1} (g_0'') +$$

$$\frac{(d_0 W)^{1-n} |g_0'|^{2-n}}{n-1} \left[f_0' g_0' - c_0 \Lambda \left(f_0'' g_0 + f_0' g_0' \right) \right] = 0 \quad as \quad \eta \to \infty \tag{3.7}$$

Solving this quadratic leads to:

$$g_0'' = \frac{0.5}{n-1} - (d_0 W)^{1-n} |g_0'|^{2-n} f_0 \pm$$

$$\sqrt{(d_0 W)^{2-2n} |g_0'|^{4-2n} f_0^2 - 4 (d_0 W)^{1-n} |g_0'|^{2-n} (n-1) \left[f_0' g_0' - c_0 \Lambda \left(f_0'' g_0 + f_0' g_0' \right) \right]} \tag{3.8}$$

As before, the negative sign in front of the square root function is chosen. Equations (3.5) and (3.8) will be used in the solution for dilatant fluids in section 3.2.4.

The values of n selected for this study are based on physical models of fluids as listed in Table 3.1. These values of n correspond to values of n in Kim [9], Lee et al. [8], and Kleingstreuer et al. [11] used in the comparisons which follow. The lower limit of Λ was chosen to remain ahead of the separation point of the flow, where laminar boundary layer analysis becomes meaningless. The upper limits of Λ were derived to stay just behind the forward stagnation point for a sphere as determined by:

$$\Lambda = \frac{\dfrac{n+1}{R} \cos\dfrac{x}{R} \displaystyle\int_0^x \left(\sin\dfrac{x}{R} \right)^{3n} dx}{\left(\sin\dfrac{x}{R} \right)^{3n+1}} \tag{3.9}$$

which is Equation (2.14) evaluated for a sphere with,

$$\frac{r}{R} = \sin\frac{x}{R}\,, \qquad \frac{U_e}{U_\infty} = \frac{3}{2}\sin\frac{x}{R} \qquad where\ \ L = R \qquad (3.10a,b)$$

Λ_{max} is determined by applying L'Hospital's Rule to Equation (3.9) and then setting R to unity and x to zero.

Table 3.1 The physical models of the selected n's.

n	Range of Λ	Physical Model
0.229	0.1 - 0.5	23.3% Illinois Yellow Clay in Water
0.520	0.1 - 0.5	0.67% CMC in Water
0.600	0.1 - 0.5	CMC in Water
0.716	0.1 - 0.5	10% Napalm in Kerosene
1.000	0.1 - 0.5	Newtonian Fluid
1.200	0.1 - 0.45	Ethylene Oxide in NaCl solution
1.400	0.1 - 0.45	Ethylene Oxide in NaCl solution
1.600	0.1 - 0.44	Ethylene Oxide in NaCl solution

3.1 Numerical Integration

The differential equations are integrated using a fourth order Runge-Kutta formula:

$$y_{j+1} = y_j + \frac{1}{6}(k_1 + 2k_2 + 2k_3 + k_4)$$

$$\begin{aligned}
\textit{Defining:}\quad k_1 &= hf(x_j, y_j)\\
k_2 &= hf\left(x_j+\frac{h}{2}, y_j+\frac{k_1}{2}\right)\\
k_3 &= hf\left(x_j+\frac{h}{2}, y_j+\frac{k_2}{2}\right)\\
k_4 &= hf(x_j+h, y_j+k_3)\\
h &= \Delta\eta
\end{aligned} \tag{3.11}$$

The Runge-Kutta method has the advantages of being a self-starting, simple, yet accurate procedure to solve ordinary differential equations. A disadvantage is the need to evaluate intermediate derivatives to achieve the solution. This led to significant computing time that was, however, not insurmountable. The f_o and g_o equations are expressed as follows in a computer program:

$$\begin{aligned}
F(1) &= f_0(\Lambda, \eta)\\
F(2) &= f_0'(\Lambda, \eta)\\
F(3) &= f_0''(\Lambda, \eta)\\
F(4) &= g_0(\Lambda, \eta)\\
F(5) &= g_0'(\Lambda, \eta)
\end{aligned} \tag{3.10}$$

Denoting the derivative with *'D'* creates;

$$\begin{aligned}
DF(1) &= f_0'(\Lambda, \eta) = F(2)\\
DF(2) &= f_0''(\Lambda, \eta) = F(3)\\
DF(3) &= -F(1)*F(3)*DABS(F(3))**(1.0D0-NN)-LAMDA*\\
&\quad DABS(F(3))**(1.0D0-NN)*(1-F(2)*F(2)+B0*\\
&\quad W*W*F(4)*F(4)) \qquad (3.11)\\
DF(4) &= g_0'(\Lambda, \eta) = F(5)\\
DF(5) &= -(W*DI0)**(1.0D0-NN)*DABS(F(5))**(1.0D0-\\
&\quad NN)*(F(1)*F(5)-C0*LAMDA*F(2)*F(4))
\end{aligned}$$

The applicable boundary conditions are F(1)=F(2)=0, F(4)=1 @ η=0; and F(2)=1, F(4)=0 @ $\eta \rightarrow \infty$. Additionally, two asymptotic boundary conditions are required; F(3)=F(5)=0 @$\eta \rightarrow \infty$. The solution is pursued as an initial value problem necessitating the initial values of F(3) and F(5), such that the differential equations satisfy the remaining asymptotic boundary conditions.

The exact values of F(3) and F(5) can not be determined or 'guessed' effectively, therefore requiring an iterative solution. The iteration applied combines the tested Newton-Raphson technique with the Least-squares evaluation of the error. The Newton-Raphson procedure requires additional differential equations obtained from differentiating the original differential equations with respect to the initial conditions. These perturbation equations are evaluated with the original equations.

Defining $f_o''(0)$ as x and $g_o'(0)$ as y, and using a Taylor series, the end boundary conditions become;

$$1 - f_0' + f_{0x}' \Delta x + f_{0y}' \Delta y \ , \quad 0 - g_0 + g_{0x} \Delta x + g_{0y} \Delta y \qquad (3.12a,b)$$

accompanied with the asymptotic boundary conditions of

$$0 - f_0'' + f_{0x}'' \Delta x + f_{0y}'' \Delta y \ , \quad 0 - g_0' + g_{0x}' \Delta x + g_{0y}' \Delta y \quad \eta - \eta_\infty \qquad (3.13a,b)$$

where M_x and M_y denote $\partial/\partial x$ and $\partial/\partial y$ respectively.

The values $M_x \Delta x$ and $M_y \Delta y$ represent the changes in M due to a small change, Δx or Δy, in x and y. The errors between the RHS and LHS of Equations (3.12) and (3.13) become;

$$
\begin{aligned}
\delta_1 &= f'_{0x}\Delta x + f'_{0y}\Delta y + (f'_0 - 1) \\
\delta_2 &= g_{0x}\Delta x + g_{0y}\Delta y + g_0 \\
\delta_3 &= f''_{0x}\Delta x + f''_{0y}\Delta y + f''_0 \\
\delta_4 &= g'_{0x}\Delta x + g'_{0y}\Delta y + g'_0
\end{aligned}
\tag{3.14}
$$

These are minimized using the Least-square method, ultimately leading to the corrections Δx and Δy:

$$
\Delta x = \frac{\Delta xNUM}{DEN}\ , \qquad \Delta y = \frac{\Delta yNUM}{DEN} \tag{3.15a,b}
$$

where:

$$
\begin{aligned}
\Delta xNUM = {} & -\left[f'_{0x}(f'_0-1) + g_{0x}g_0 + f''_{0x}f''_0 + g'_{0x}g'_0\right]\left[f^2 + g^2_{0y} + f^2 + g^2\right] + \\
& \left[f'_{0y}(f'_0-1) + g_{0y}g_0 + f''_{0y}f''_0 + g'_{0y}g'_0\right]\left[f'_{0x}f'_{0y} + g_{0x}g_{0y} + f''_{0x}f''_{0y} + g'_{0x}g'_{0y}\right] \\
\Delta yNUM = {} & \left[f'_{0x}f'_{0y} + g_{0x}g_{0y} + f''_{0x}f''_{0y} + g'_{0x}g'_{0y}\right]\left[f'_{0x}(f'_0-1) + g_{0x}g_0 + f''_{0x}f''_0 + g'_{0x}g'_0\right] - \\
& \left[f^2 + g^2_{0x} + f^2 + g^2\right]\left[f'_{0y}(f'_0-1) + g_{0y}g_0 + f''_{0y}f''_0 + g'_{0y}g'_0\right] \\
DEN = {} & \left[f'_{0x}g_{0y} - g_{0x}f'_{0y}\right]^2 + \left[f'_{0x}f''_{0y} - f''_{0x}f'_{0y}\right]^2 + \left[f'_{0x}g'_{0y} - g'_{0x}f'_{0y}\right]^2 + \\
& \left[g_{0x}f''_{0y} - f''_{0x}g_{0y}\right]^2 + \left[g_{0x}g'_{0y} - g'_{0x}g_{0y}\right]^2 + \left[f''_{0x}g'_{0y} - g'_{0x}f''_{0y}\right]^2
\end{aligned}
\tag{3.15c,d,e}
$$

The partial derivatives with respect to the initial conditions, M_x and M_y, are determined by integrating the following perturbation equations;

$$
\begin{aligned}
F(6) &= f_{0x}(\Lambda,\eta) & \qquad F(11) &= f_{0y}(\Lambda,\eta) \\
F(7) &= f'_{0x}(\Lambda,\eta) & \qquad F(12) &= f'_{0y}(\Lambda,\eta) \\
F(8) &= f''_{0x}(\Lambda,\eta) & \qquad F(13) &= f''_{0y}(\Lambda,\eta) \\
F(9) &= g_{0x}(\Lambda,\eta) & \qquad F(14) &= g_{0y}(\Lambda,\eta)
\end{aligned}
$$

$$F(10) = g'_{0x}(\Lambda,\eta) \qquad F(15) = g'_{0y}(\Lambda,\eta) \qquad (3.16)$$

```
DF(6) = F(7)
DF(7) = F(8)
DF(8) = -DABS(F(3))**(1.0D0-NN)*(F(6)*F(3)+F(1)*F(8)-
        2.0D0*LAMDA*(F(2)*F(7)-B0*W*F(4)*F(9)))-(1.0D0-
        NN)*DABS(F(3))**(-NN)*F(8)*(F(1)*F(3)+LAMDA*
        (1.0D0-F(2)*F(2)+B0*W*W*F(4)*F(4)))
DF(9) = F(10)
DF(10) = (W*DI0)**(1.0D0-NN)*((1.0D0-NN)*DABS(F(5))**
        (-NN)*(F(10))*(C0*LAMDA*F(2)*F(4)-F(1)*F(5))+
        DABS(F(5))**(1.0D0-NN)*(C0*LAMDA*(F(7)*F(4)+
        F(2)*F(9))-F(6)*F(5)-F(1)*F(10)))
DF(11) = F(12)
DF(12) = F(13)

DF(13) = -DABS(F(3))**(1.0D0-NN)*(F(11)*F(3)+F(1)*
        F(13)-2.0D0*LAMDA*(F(2)*F(12)-B0*W*W*F(4)*
        F(14)))-(1.0D0-NN)*DABS(F(3))**(-NN)*F(13)*
        (F(1)*F(3)+LAMDA*(1.0D0-F(2)*F(2)+B0*W*W*
        F(4)*F(4)))
DF(14) = F(15)
DF(15) = (W*DI0)**(1.0D0-NN)*((1.0D0-NN)*DABS(F(5))**
        (-NN)*(-F(15))*(C0*LAMDA*F(2)*F(4)-F(1)*F(5))+
        DABS(F(5))**(1.0D0-NN)*(C0*LAMDA*(F(12)*F(4)+
        F(2)*F(14))-F(11)*F(5)-F(1)*F(15)))
```

with the initial conditions,

$$F(6)=F(7)=F(9)=F(10)=$$
$$F(11)=F(12)=F(13)=F(14)=0$$
$$F(8)=F(15)=1 \qquad @\ \eta=0 \qquad (3.17)$$

While the above correction technique can be quite effective in leading the solution to convergence, the initial estimates for x and y need to be somewhat close to the actual values. If not, the solution diverges rapidly. A method to avoid this situation is to initially choose a limiting value for η_∞. This will lead to a 'rough' first solution for x and y. Then using these values for $f_o(0)''$ and $g_o(0)'$, η_∞ is extended out to its ultimate value.

As discussed in Section 2.3, f_o'' is greater than or equal to zero, therefore $|f_o''|$ equals f_o'' or DABS(F(3))= F(3), DABS(F(8))=F(8), and DABS(F(13))=F(13). Likewise, with g_o' less than zero, $|g_o'|$ equals $-g_o'$, or DABS(F(5))=-F(5), DABS(F(10))=-F(10), and DABS(F(15))=-F(15).

Termination of the numerical analysis is controlled in the program by monitoring two variables *TEST* and *ETEST*. Values for these controllers are set within the input data statements, and range from 10^{-3} to 10^{-11} for $n=1.6$ to $n=0.229$, respectively. *TEST* terminates the calculation based on the incremental change in x and y, or the initial conditions. *ETEST* is compared to the sum of the squares of the differences *(errors)* between the boundary conditions at η_∞ and the calculated values at η_∞, or E, which is defined as;

$$E = (1-f_0'(\Lambda,\eta))^2 + (f_0''(\Lambda,\eta))^2 + (g_0(\Lambda,\eta))^2 + (g_0'(\Lambda,\eta))^2 \quad (3.18)$$

When E is minimized below *ETEST*, after the *TEST* criteria is met, programming is halted. *ETEST* is the limiting factor for the accuracy of the calculations. Assuming each error contributes an equivalent portion to the total error, each is assumed to maintain an accuracy equal to $(E/4)^{1/2}$. Therefore if $E=10^{-9}$ each error is;

$$1-f_0'(\Lambda,\eta_\infty) = f_0''(\Lambda,\eta_\infty) = g_0(\Lambda,\eta_\infty) = g_0'(\Lambda,\eta_\infty) = 1.581138x10^{-5} \tag{3.19}$$

For the non-rotational analysis with $g_o=g_o'=0$,

$$E = (1-f_0'(\Lambda,\eta_\infty))^2 + (f_0''(\Lambda,\eta_\infty))^2 \tag{3.20}$$

and again assuming $E=10^{-9}$, each error becomes;

$$1-f_0'(\Lambda,\eta_\infty) = f_0''(\Lambda,\eta_\infty) = 2.36067x10^{-5} \tag{3.21}$$

3.2 Numerical Solutions of f_o and g_o Equations and Their Accuracy

The Fortran program developed for this analysis is intended to determine the boundary layer developing over non-rotating and rotating axisymmetrical bodies in Newtonian and Power-law fluids. The geometric parameters b_o, c_o, d_o define the body studied, which in this analysis is a sphere. While this diverges from the previous "seed" work, Kim [9], where the solution is in universal format, it follows the work done by other authors within the realm of a rotating body.

The previous work found the integration step-size, $\Delta\eta$, to be the most important controlling factor for a fairly quick and accurate solution. This analysis found with increasing rotation velocity, increasing rotation parameter W, the solution increased in difficulty and decreased significantly in accuracy. The fluids most dramatically effected were dilatant. Some of which at the greater values of n and W were not solved in this analysis.

The evaluation of the results is separated first into non-rotating and rotating groups. The rotating solutions are further subdivided by fluid type, i.e., Newtonian, Pseudo-plastic, and Dilatant.

3.2.1 Non-Rotating; Newtonian and Power-Law Fluids

The first area to confirm proper program performance is for the non-rotating sphere, or $W=0$. Adjustments in the subroutine *'DIFF'* were required for all derivatives that contained W raised to a power, which include DF(5), DF(10), and DF(15). When $W=0$, these derivatives are set to zero. The integration step size, $\Delta\eta$, was maintained at 10^{-2} for all of the calculations. *ETEST* varied from 10^{-9} for pseudo-plastics to 10^{-10} for dilatant fluids.

The value of $f_o''(\Lambda,0)$ for $n=0.229$, 0.520, 0.716, 1.200, and 1.600, with $\Lambda=0.0$ and 1.0 are presented in Table

3.2 along with a comparison of results from Kim [9]. All results are equivalent for at least the first six significant digits except for $n=0.229$, $\Lambda=0.000$. This discrepancy could be due to the exceedingly larger value of η_∞ used, 1600 in this analysis versus 400 in Kim. In all calculations the value of η_∞ was larger than the reference value, however not to this extent. The degree of correlation between this analysis and Kim demonstrates that the extended analysis to include body rotation has not effected non-rotational calculations, which is as expected.

Table 3.2 Comparison of $f_o''(0)$ with published data for non-rotating bodies, $W=0$.

		Present		Kim [9]
n	Λ	$f_o''(0)$	η_∞	$f_o''(0)$
0.229	1.000	0.92219907	400	0.9221991
	0.000	0.15854029	1600	0.1585939
0.520	1.000	1.0865653	284	1.08656532
	0.000	0.28193441	475	0.28193462
0.716	1.000	1.1603653	54	1.16036533
	0.000	0.36313748	79	0.36313757
1.200	1.000	1.2664192	3.2	1.26641921
	0.000	0.53506325	3.766	0.53506307
1.600	1.000	1.3074728	1.8302	1.3074729
	0.000	0.64338603	2.3497	0.6433860

3.2.2 Rotating Sphere; Newtonian Fluids

The value of $\Delta\eta=0.02$ is capable of maintaining a total accumulated error, E, of 10^{-9} for all values of Λ and W studied. Differing from previous work where η_∞ was limited for various reasons, this analysis let η_∞ *'float'* until $E \leq 10^{-9}$ was achieved. The values of W=1.5, 3.0, and 4.7434 correspond to B=1, 4, and 10 from Lee, et al.[8], to which the present solutions of $f_o''(0)$ and $g_o'(0)$ are compared in Table 3.3. As can be seen, correlation is excellent with all values being equivalent to Lee's $f_o''(0)$ and $g_o'(0)$ values.

There is an associated decrease in η_∞ as W increases representing a compression of the boundary layer thickness with an increase in the rotational velocity. Increasing W from 1.5 to 3.0 decreases η_∞ by 5.23% on the average; going from W=3.0 to 4.7434 decreases η_∞ 3.33%. Also with an increasing W, $g_o'(0)$ or the tangential velocity gradient increases. Both of these factors indicate a *'shear thinning'* which is indicative of non-Newtonian fluids.

The linear velocity profiles, f_o' versus η and g_o versus η for the calculated Λ's are shown in Figures 3.1, 3.2, 3.3 for W=1.5, 3.0, and 4.7434, respectively.

Table 3.3 Comparison of $f_o''(0)$ and $g_o'(0)$ with published data for Newtonian Fluids, n=1.

		Present			Lee, et al. [8]	
W	Λ	$f_o''(0)$	$g_o'(0)$	η_∞	$f_o''(0)$	$g_o'(0)$
1.5	0.50	1.112929	-0.784888	7.00	1.1129	-0.7849
	0.40	1.013919	-0.732034	7.10	1.0139	-0.7320
	0.30	0.905123	-0.675397	7.12	0.9051	-0.6754
	0.20	0.783143	-0.614028	7.14	0.7831	-0.6140
	0.10	0.642062	-0.546405	7.18	0.6421	-0.5464
3.0	0.50	1.623264	-0.846287	6.56	1.6233	-0.8463
	0.40	1.454850	-0.785636	6.76	1.4549	-0.7856
	0.30	1.267449	-0.720138	6.78	1.2675	-0.7201
	0.20	1.053568	-0.648280	7.00	1.0536	-0.6483
	0.10	0.799146	-0.567204	7.12	0.7992	-0.5673
4.7	0.50	2.521634	-0.936148	6.40	2.5216	-0.9362
	0.40	2.233815	-0.864939	6.48	2.2338	-0.8649
	0.30	1.911136	-0.787437	6.56	1.9111	-0.7874
	0.20	1.538800	-0.701286	6.72	1.5388	-0.7013
	0.10	1.087341	-0.601462	6.92	1.0873	-0.6015

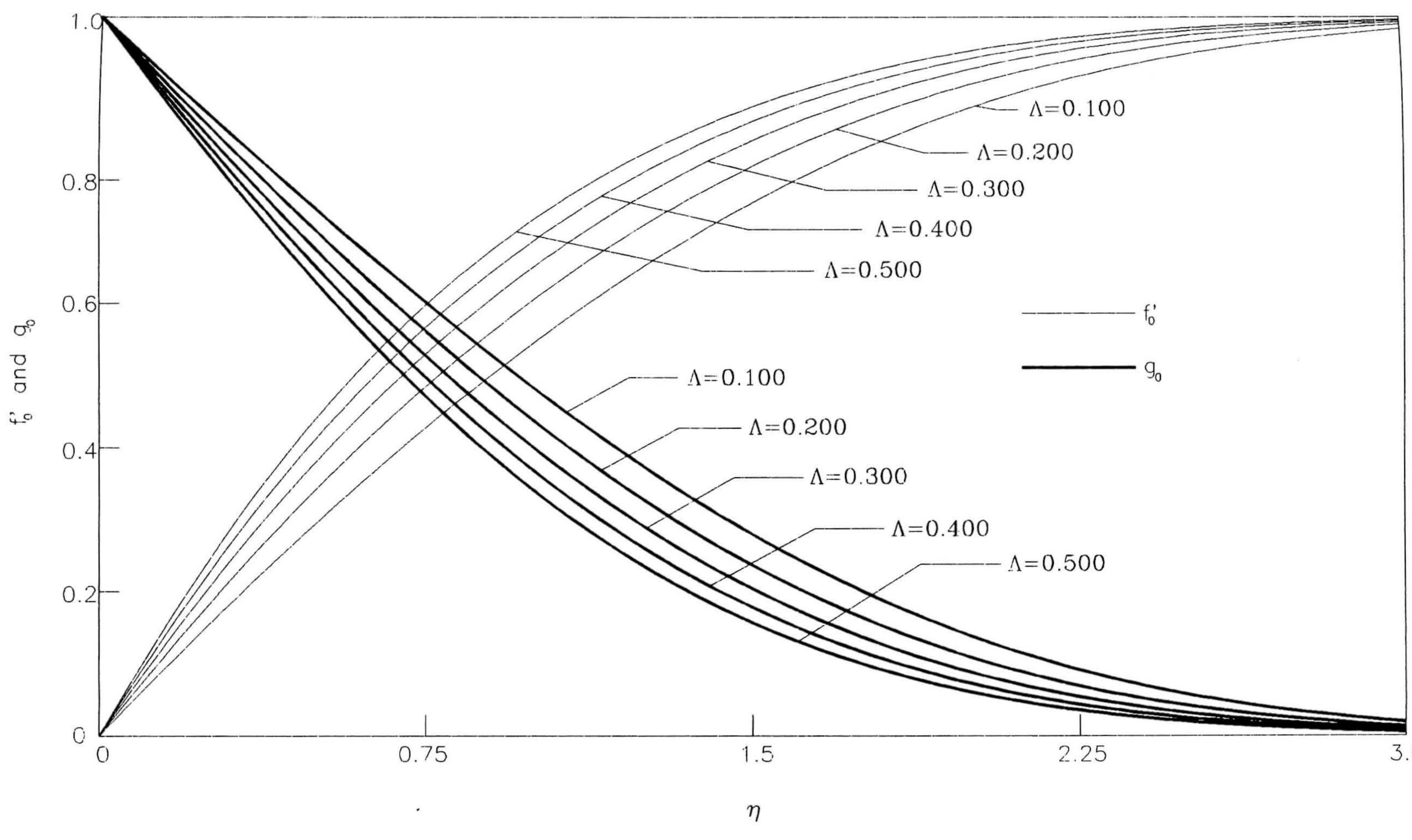

Fig. 3.1 f_0' and g_0 vs. η for n=1.00 and W=1.5

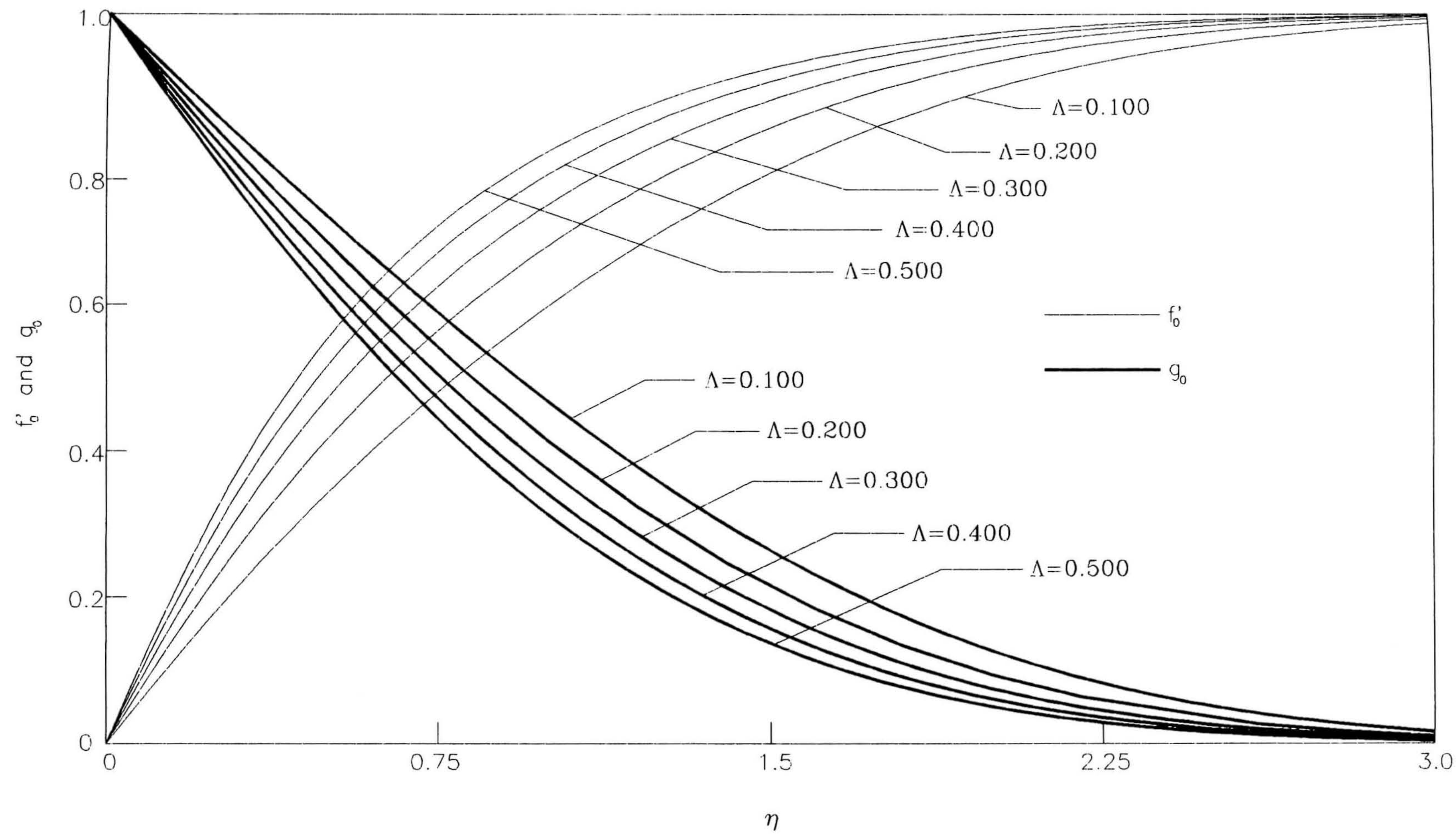

Fig. 3.2 f_0' and g_0 vs. η for n=1.00 and W=3.0

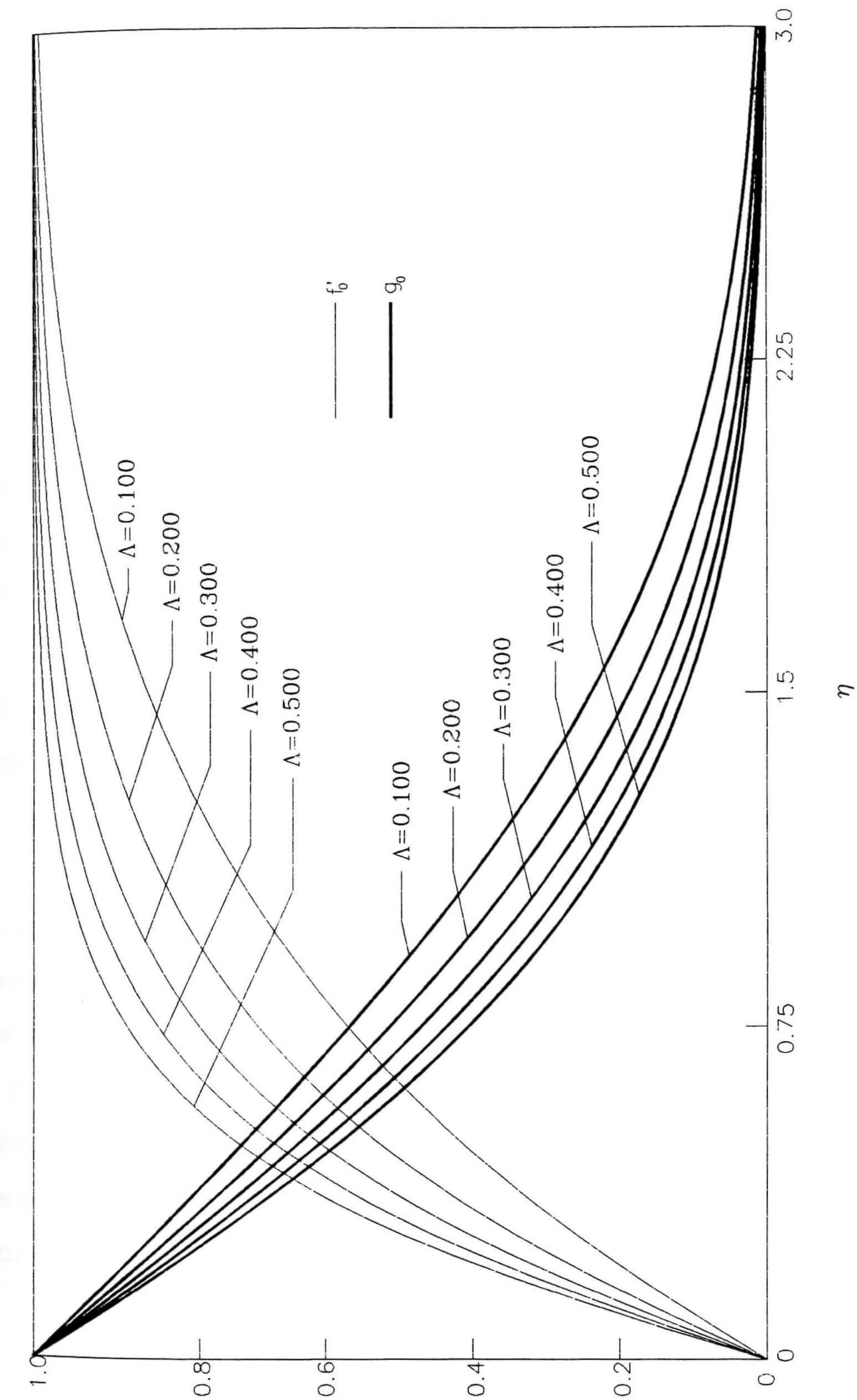

Fig. 3.3 f_0' and g_0 vs. η for n=1.00 and W=4.7434

3.2.3 Rotating Sphere; Pseudo-Plastic Fluids

The analysis of Pseudo-plastic fluids shows a significant increase in η_∞ as n decreases. Maintaining the same accumulated error value of 10^{-9}, at n=0.229 and Λ=0.100, η grows to $\eta_\infty=9500$. It may be noted that the increment of η_∞ does not necessarily reflect the proportional increment of the actual boundary layer thickness. Nevertheless, this subsequent increase to η_∞ likewise leads to a tremendous increase in the computational time for the solution. While lowering *'E'* would reduce the computing time and the output file size, it was decided to adjust the printing interval and run as many of the calculations as possible on thefastest computer available. Discussion of the computing time is reviewed in a later section.

Therefore with *'E'* set at 10^{-9}, $\Delta\eta$ can remain initially at 0.02 for n=0.716 and n=0.520, however due to the large increase in η_∞ for n=0.229, $\Delta\eta$ is increased to 0.04. A comparison analysis was made with $\Delta\eta$=0.02 and an equivalent η_∞. The final results for $f_o''(0)$ and $g_o'(0)$ were equal regardless of $\Delta\eta$=0.02, or $\Delta\eta$=0.04, therefore 0.04 was chosen to reduce the computation time. The following summarizes the constraints for this analysis of Pseudo-plastic fluids,

n=0.716:

$$\begin{aligned} &E=10^{-9} \\ &\Delta\eta=0.02 \quad 0\le\eta\le 8 \\ &\quad\ =0.20 \quad 8\le\eta\le 80 \end{aligned} \qquad (3.22a)$$

n=0.520:

$$
\begin{aligned}
&E=10^{-9} \\
&\Delta\eta=0.02 \quad 0\leq\eta\leq 8 \\
&\quad =0.20 \quad 8\leq\eta\leq 80 \\
&\quad =2.00 \quad 80\leq\eta\leq\eta_\infty
\end{aligned}
\tag{3.22b}
$$

n=0.229:

$$
\begin{aligned}
&E=10^{-9} \\
&\Delta\eta=0.04 \quad 0\leq\eta\leq 8 \\
&\quad =0.40 \quad 8\leq\eta\leq 80 \\
&\quad =4.00 \quad 80\leq\eta\leq 800 \\
&\quad =40.00 \quad 800\leq\eta\leq 8000 \\
&\quad =400.0 \quad 8000\leq\eta\leq\eta_\infty
\end{aligned}
\tag{3.22c}
$$

The results of $f_o''(0)$ and $g_o'(0)$ for the three values of n and W=1.5, 3.0, and 4.7434 are listed in Tables 3.4, 3.5, and 3.6. Graphical representation of f_o' versus η and g_o versus η for n=0.520 and all three values of W are shown in Figures 3.4 through 3.6.

As with Newtonian fluids, Pseudo-plastics have the characteristic of *'shear thinning'*. The tangential velocity gradient, $g_o'(\eta)$, increases with increasing values of W, and η_∞ decreases for respective Λ's as can be seen by the tabulated data.

3.2.4 Rotating Sphere; Dilatant Fluids

Reviewing η, η_∞ is anticipated to decrease with an increasing value of n. This is accompanied with a steep slope to the $f_o''(0)$ and $g_o'(0)$ functions and quick approach to the asymptotic boundary conditions. In an effort to adjust to this change in the derivatives, *'SAVETA'* is employed to

Table 3.4 $f_o''(0)$ and $g_o'(0)$ for Pseudo-Plastic Fluids, n=0.229.

		Present		
W	Λ	$f_o''(0)$	$g_o'(0)$	η_∞
1.5	0.500	0.786687	-0.439756	7000
	0.400	0.670010	-0.387001	8144
	0.300	0.549476	-0.332846	8292
	0.200	0.424391	-0.277048	8600
	0.100	0.294049	-0.219232	9500
3.0	0.500	1.375743	-0.674187	2962
	0.400	1.145536	-0.588120	3352
	0.300	0.908008	-0.499461	6000
	0.200	0.662520	-0.407588	8070
	0.100	0.409870	-0.311317	9200
4.74	0.500	2.588564	-0.970026	4350
	0.400	2.118904	-0.839389	5550
	0.300	1.635279	-0.704368	6380
	0.200	1.137964	-0.563646	7950
	0.100	0.633293	-0.414369	9100

Table 3.5 $f_o''(0)$ and $g_o'(0)$ for Pseudo-Plastic Fluids, n=0.520.

		Present		
W	Λ	$f_o''(0)$	$g_o'(0)$	η_∞
1.5	0.500	0.952621	-0.598083	384
	0.400	0.839308	-0.542213	424
	0.300	0.718489	-0.483538	464
	0.200	0.588016	-0.421430	500
	0.100	0.444498	-0.354899	540
3.0	0.500	1.526668	-0.774958	342
	0.400	1.318723	-0.697810	352
	0.300	1.095894	-0.616316	370
	0.200	0.853871	-0.529243	408
	0.100	0.586059	-0.434301	502
4.74	0.500	2.625123	-0.984490	308
	0.400	2.234716	-0.880772	328
	0.300	1.815326	-0.770578	344
	0.200	1.358686	-0.651692	368
	0.100	0.852711	-0.519428	394

Table 3.6 $f_o''(0)$ and $g_o'(0)$ for Pseudo-Plastic Fluids, n=0.716.

		Present		
W	Λ	$f_o''(0)$	$g_o'(0)$	η_∞
1.5	0.500	1.031469	-0.684597	46.6
	0.400	0.923501	-0.629252	50.6
	0.300	0.806693	-0.570547	54.6
	0.200	0.678235	-0.507681	57.2
	0.100	0.533434	-0.439383	58.2
3.0	0.500	1.581847	-0.814367	45.9
	0.400	1.390666	-0.744214	49.9
	0.300	1.182080	-0.669294	53.3
	0.200	0.950105	-0.588184	54.6
	0.100	0.684403	-0.498238	55.7
4.74	0.500	2.595241	-0.970258	39.5
	0.400	2.251562	-0.881685	40.0
	0.300	1.874770	-0.786440	40.5
	0.200	1.453026	-0.682133	41.0
	0.100	0.965328	-0.563690	41.6

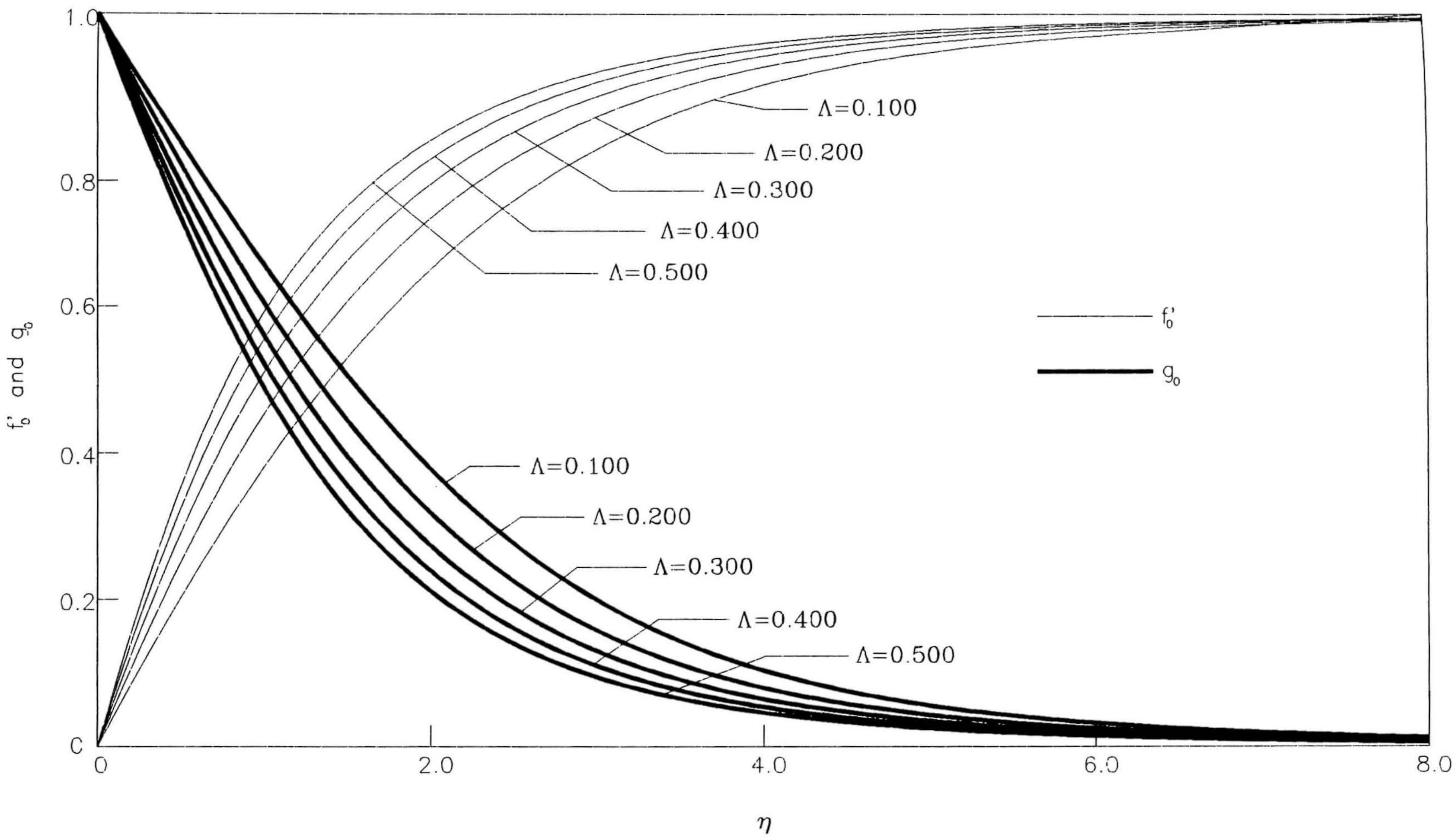

Fig. 3.4 f_0' and g_0 vs. η for n=0.520 and W=1.5

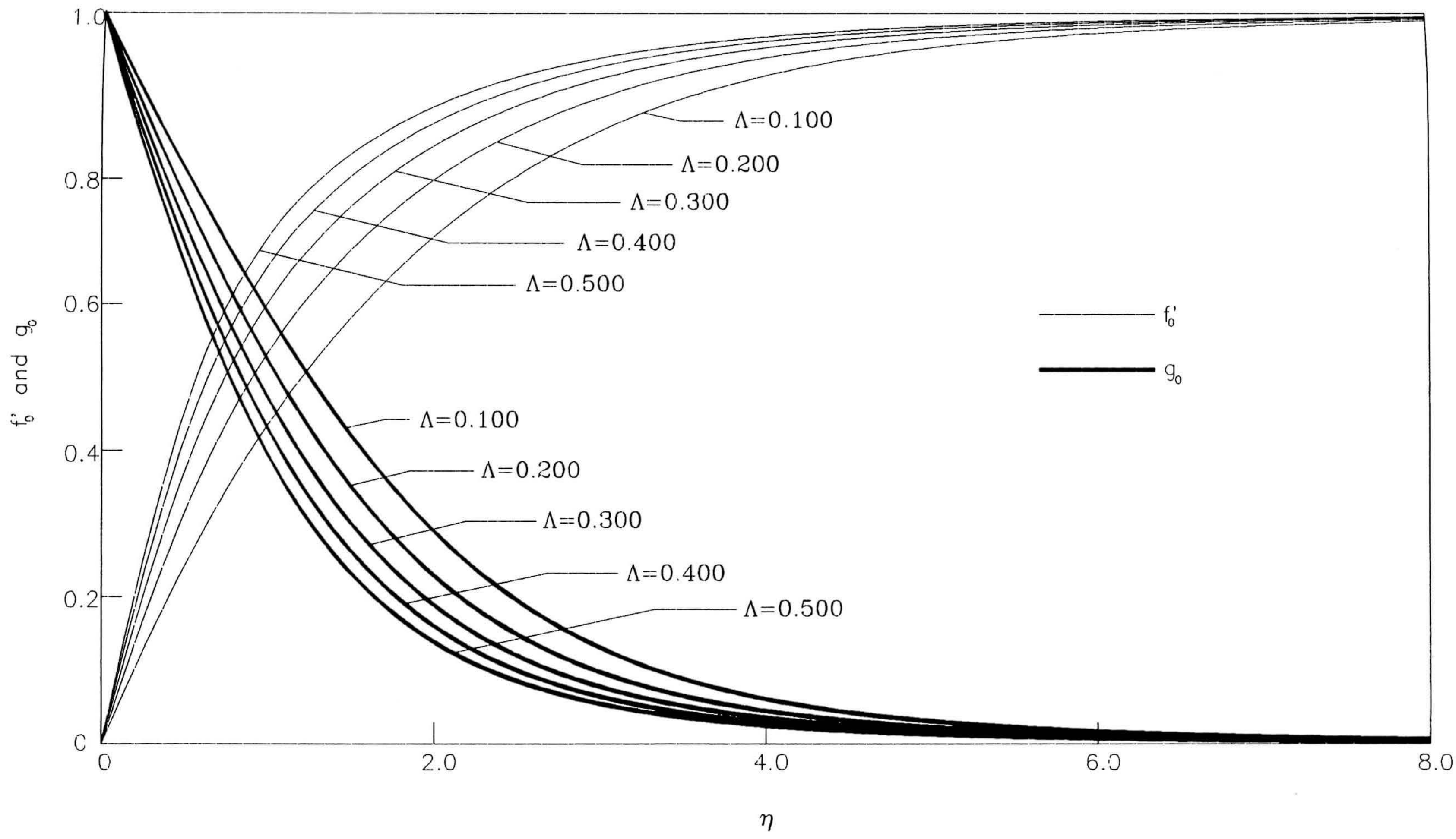

Fig. 3.5 f_c' and g_o vs. η for n=0.520 and W=3.0

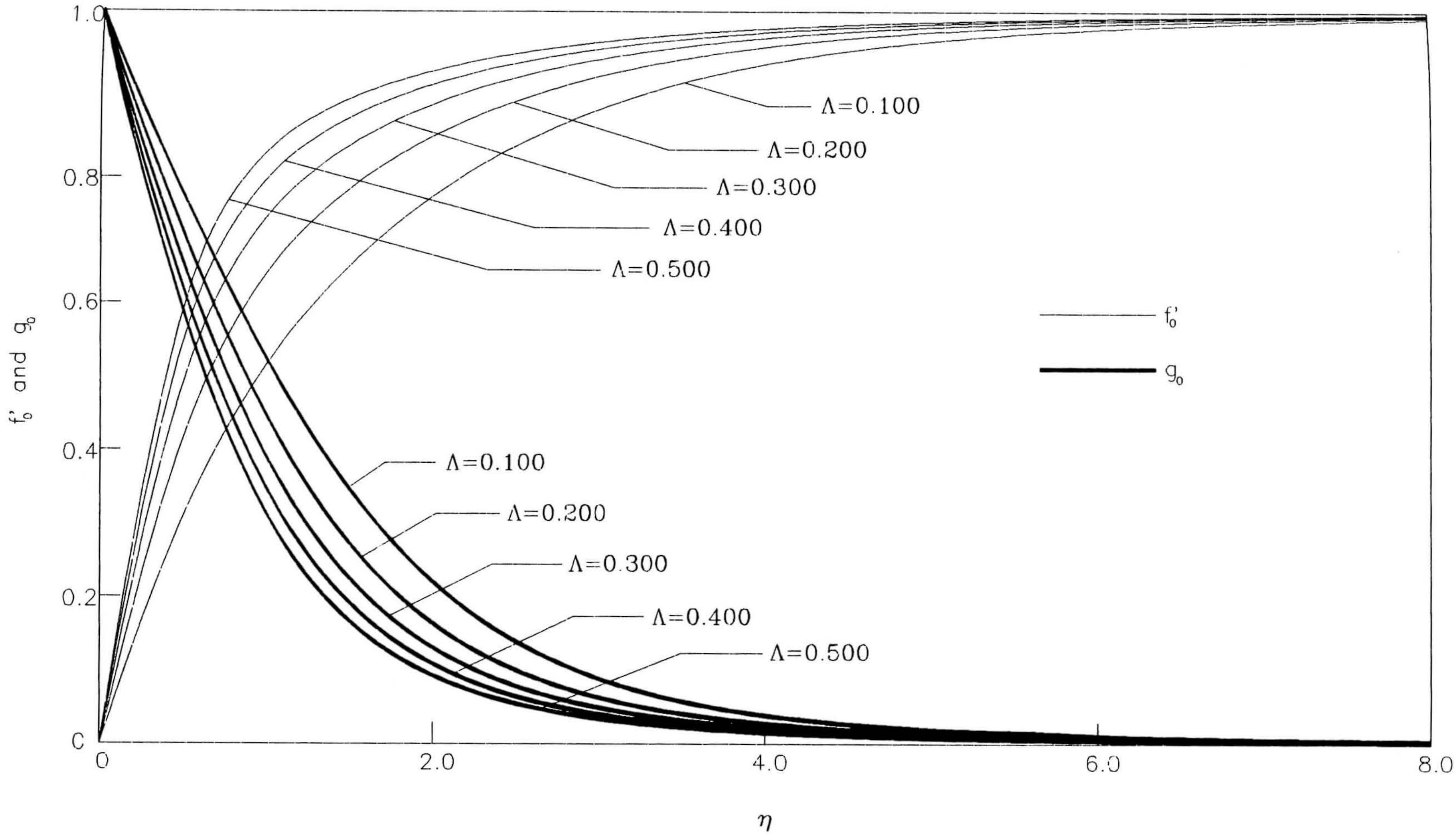

Fig. 3.6 f_0' and g_0 vs. η for n=0.520 and W=4.7434

reduce the size of $\Delta\eta$ near η_∞ [9]. The actual value of *'SAVETA'* varies with n, Λ, and the respective η_∞. The choice of *'SAVETA'* and η_∞ for the first calculated Λ, of each combination of n and W, is the most time consuming process, taking at times hours to conclude on a personal computer. Subsequent values of Λ took less time to compute, however hour(s) were still the time-measure for completion. *'E'* varies the most for dilatant fluids, requiring a reduction of its value with increasing values of n and W.

As previously mentioned, $f_o'''(\eta)$ and $g_o''(\eta)$ become uncalculable as η approaches η_∞ due to the negative power of the apparent viscosity term. This is circumvented by applying L'Hospital's Rule to the respective equations. Within the computer program, the constant *'ROPTAL'* is used to switch the calculation of $f_o'''(\eta)$ and $g_o''(\eta)$ from Equations (2.21a) and (2.21b), respectively, to Equations (3.5) and (3.8). The values of $f_o''(\eta)$ and $|1-f_o'(\eta)|$ are compared to *'ROPTAL'* to determine when to switch the calculations.

The following constraints were maintained in this analysis,

$$\begin{aligned}&n=1.200;\ W=1.5\\&\quad E=10^{-8}\\&\quad \Delta\eta=0.01 \qquad 0\le\eta\le SAVETA\\&\quad\quad =0.0001\ \ SAVETA<\eta\le\eta_\infty\\&\quad ROPTAL=10^{-5}\end{aligned} \tag{3.23a}$$

$$\begin{aligned}&n=1.200;\ W=3.0\\&\quad E=10^{-4}\\&\quad \Delta\eta=0.01 \qquad 0\le\eta\le SAVETA\\&\quad\quad =0.0001\ \ SAVETA<\eta\le\eta_\infty\end{aligned} \tag{3.23b}$$

$ROPTAL=10^{-3}$

n=1.400; W=1.5

$E=10^{-6}$

$$\Delta\eta=0.01 \quad 0\leq\eta\leq SAVETA \qquad (3.24a)$$
$$=0.0001 \quad SAVETA<\eta\leq\eta_{\infty}$$

$ROPTAL=10^{-4}$

n=1.400; W=3.0

$E=10^{-4}$

$$\Delta\eta=0.01 \quad 0\leq\eta\leq SAVETA \qquad (3.24b)$$
$$=0.0001 \quad SAVETA<\eta\leq\eta_{\infty}$$

$ROPTAL=10^{-4}$

n=1.600; W=1.5

$E=10^{-4}$

$$\Delta\eta=0.01 \quad 0\leq\eta\leq SAVETA \qquad (3.25a)$$
$$=0.0001 \quad SAVETA<\eta\leq\eta_{\infty}$$

$ROPTAL=10^{-3}$

n=1.600; W=3.0

$E=10^{-3}$

$$\Delta\eta=0.01 \quad 0\leq\eta\leq SAVETA \qquad (3.25b)$$
$$=0.0001 \quad SAVETA<\eta\leq\eta_{\infty}$$

$ROPTAL=10^{-3}$

Tables 3.7 and 3.8 tabulate the values of $f_o''(0)$ and $g_o'(0)$ for the three values of n and W=1.5 and 3.0. Figures 3.7 and 3.8 depict the velocity gradients f_o' and g_o versus η for n=1.400, W=1.5 and 3.0, and the calculated Λ's.

The values of η_{∞} for dilatant fluids, as seen in the tables, increase with the increase of W, whereas $g_o'(0)$ is decreasing. This is opposite to the rheological tendencies shown by the Newtonian and pseudo-plastic fluids, and is indicative of a *'shear thickening'* characteristic.

Table 3.7 $f_o''(0)$ and $g_o'(0)$ for Dilatant Fluids, W=1.5.

		Present		
n	Λ	$f_o''(0)$	$g_o'(0)$	η_∞
1.200	0.450	1.108260	-0.815998	3.220
	0.400	1.060813	-0.790278	3.260
	0.300	0.958076	-0.735815	3.345
	0.200	0.814698	-0.676434	3.453
	0.100	0.703250	-0.610540	3.582
1.400	0.450	1.141895	-0.863403	2.3940
	0.400	1.097428	-0.838894	2.4288
	0.300	1.000628	-0.786836	2.4984
	0.200	0.890046	-0.729810	2.5834
	0.100	0.758952	-0.666164	2.6903
1.600	0.440	1.159736	-0.897603	1.9786
	0.400	1.126201	-0.878874	2.0000
	0.300	1.035031	-0.829216	2.0580
	0.200	0.930123	-0.774751	2.1273
	0.100	0.804600	-0.713867	2.2130

Table 3.8 $f_o''(0)$ and $g_o'(0)$ for Dilatant Fluids, W=3.0.

		Present		
n	Λ	$f_o''(0)$	$g_o'(0)$	η_∞
1.200	0.450	1.560402	-0.830180	2.9820
	0.400	1.481248	-0.802272	3.0250
	0.300	1.307805	-0.742784	3.1104
	0.200	1.107021	-0.677080	3.1925
	0.100	0.863144	-0.602410	3.5400
1.400	0.450	1.570905	-0.836294	2.3550
	0.400	1.497816	-0.811325	2.4253
	0.300	1.336834	-0.757605	2.5580
	0.200	1.148510	-0.697682	2.6825
	0.100	0.915891	-0.628978	2.8095
1.600	0.440	0.000000	-0.000000	0.00
	0.400	0.000000	-0.000000	0.00
	0.300	0.000000	-0.000000	0.00
	0.200	1.183083	-0.708613	2.2359
	0.100	0.960582	-0.647462	2.3880

The linear and tangential velocities, f_o' and g_o, versus η for n=0.520, 1.000, 1.400, and W=1.5 and Λ=0.300 are shown in Figure 3.9. For equivalent values of W and Λ the slopes of the velocities increase with increasing values of n. Since η is dimensionless, the value of η_∞ for each n does not represent comparative boundary layer thicknesses, i.e. η=8 for n=0.520 does not mean that the boundary layer is greater than the boundary layer for n=1.400 at η=2.5.

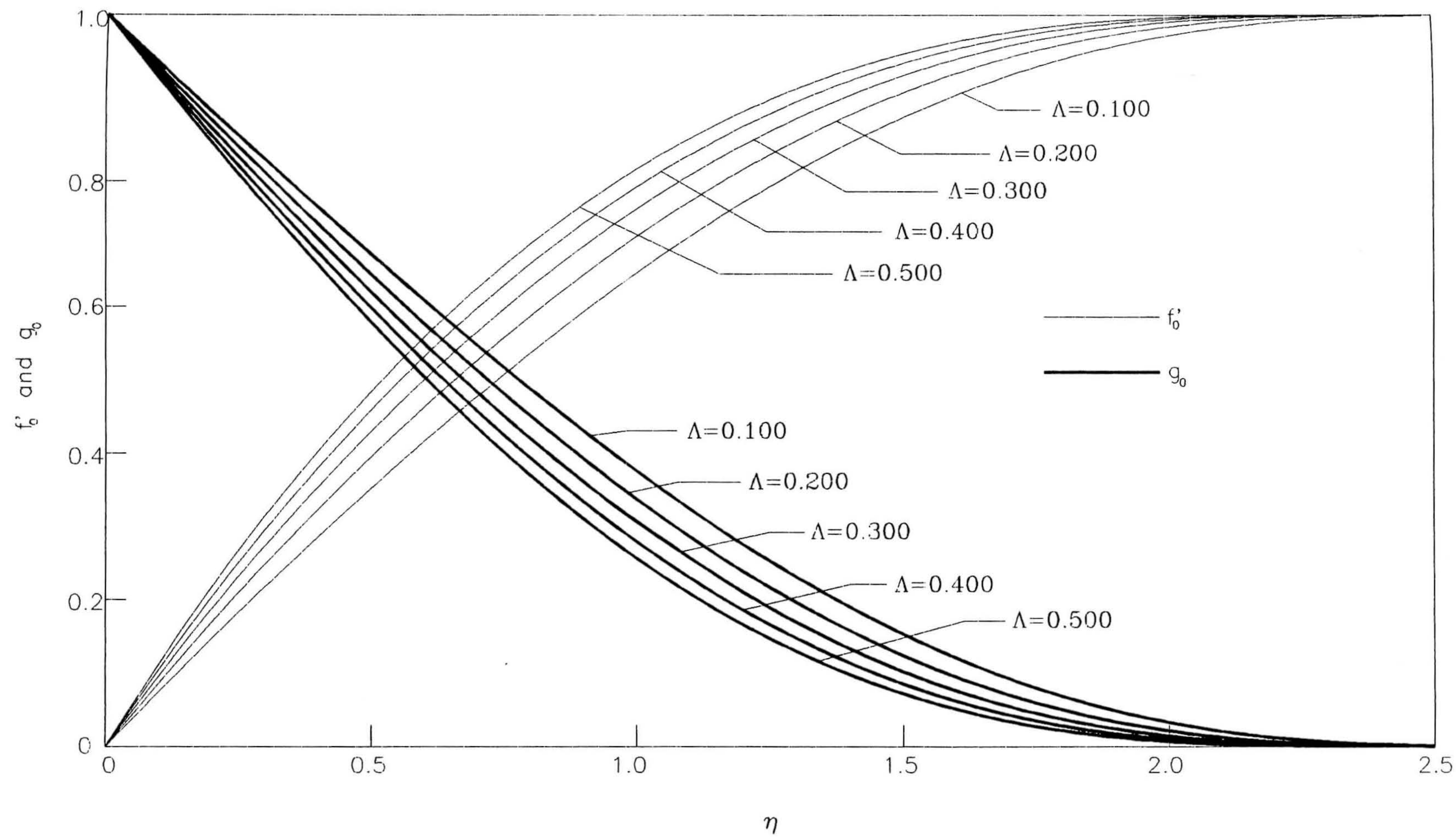

Fig. 3.7 f_0' and g_0 vs. η for $n=1.400$ and $W=1.5$

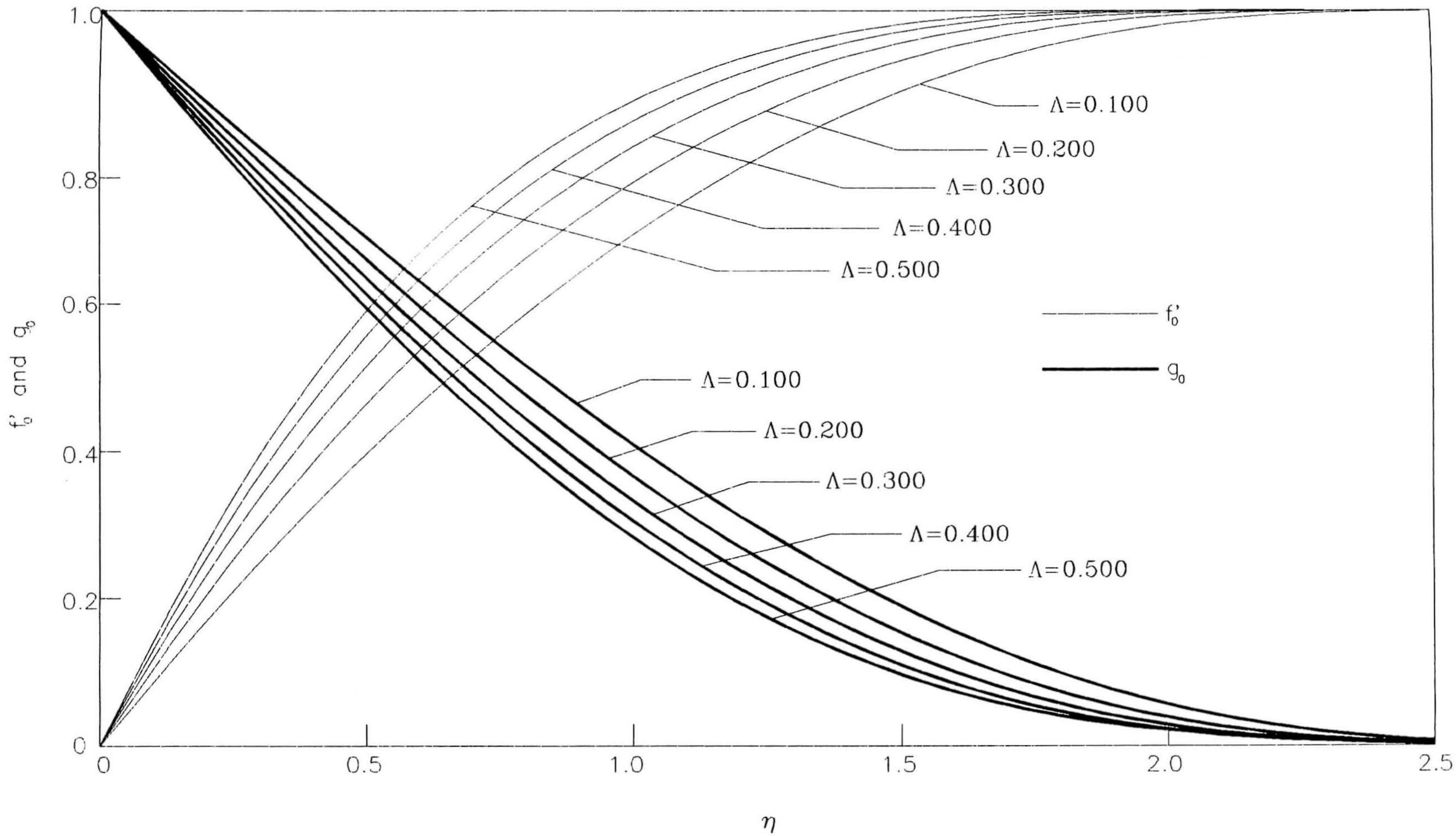

Fig. 3.8 f_0' and g_0 vs. η for n=1.400 and W=3.0

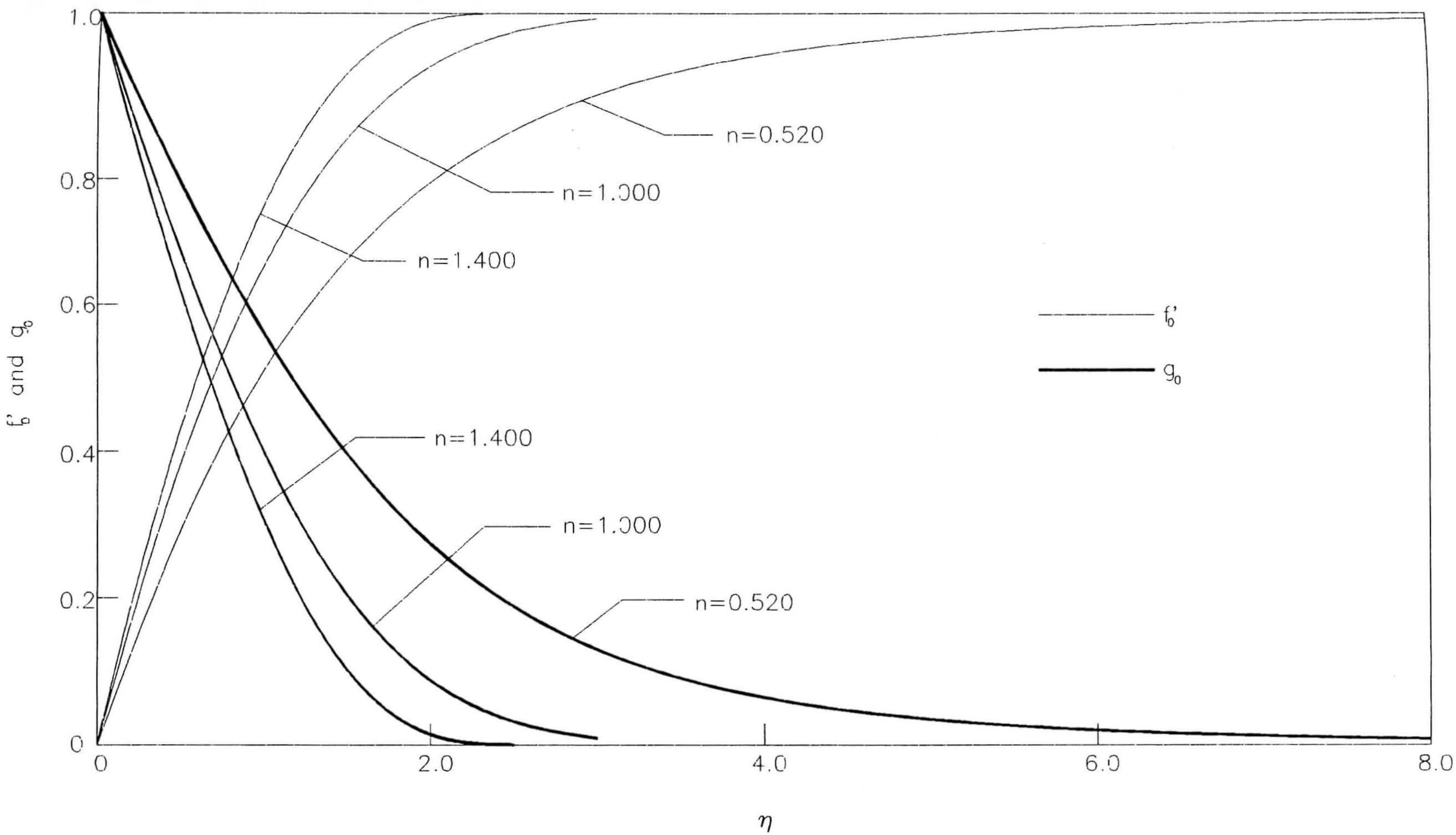

Fig. 3.9 f_0' and g_0 vs. η for n=0.520, 1.000, and 1.400, W=1.5 and $\Lambda=0.300$

3.3 Computational Time

The computational time involved in the analysis is inherently dependent on the initial estimates of $f_o''(\Lambda,0)$ and $g_o'(\Lambda,0)$, n, and W. Another factor in the time required for the analysis is the type of computer used for the calculations, i.e. personal versus mainframe. Due to the widespread availability of personal computers (PC), they were used for this study. While various PC's were accessible to the author, the two primary machines used were a 286-12Mhz and a 386-33Mhz. Table 3.9 shows the computing times for six different computers running the same set of input data: n=0.520, W=1.5, and Λ=0.100. All the computers have math co-processors installed. The data set chosen represents a medium length calculation for this analysis. As shown in the table, the 386-33Mhz computer is the fastest configuration being 17 times faster than an 8Mhz XT. A similar data set was run using the 286-12Mhz computer with and without a co-processor. The computational time without the co-processor was approximately 40 to 50 times greater than the time with a co-processor.

The program is written and compiled in Fortran utilizing IBM PC-Fortran Version 2.0. It can be compiled for computers with a math co-processor, or to emulate the presence of a co-processor for processorless computers. The fastest run times are realized with programs compiled for using the math co-processor. Input is via an input file on a floppy, harddrive, or ramdrive. The output is to another file created by the program on the same drive. The optimum results, i.e. fastest run times, are on the fastest computers utilizing a math co-processor, with the input file on a harddrive or ramdrive. A version of the program that wrote the output simultaneously to the monitor, was extremely helpful in developing the results.

Table 3.9 Computation time for various computers running data for n=0.520, W=1.500, and Λ=0.100

Computer	Processor MHz	Elapsed time Min:Sec
8088	4.33	8:23
8088	8	5:00
80286	6	6:14
80286	12	2:28
80386	25	0:54
80386	33	0:33

4.1 Wall Shear Stress

The solutions for the velocity functions can now be used to determine the local friction coefficient. Utilizing the definition of the shear stress τ_{xy} from Equation (2.5a), the coordinate transformation from Section 2.3, and the first term of the series for $f(\xi,\eta,n)$, the shear stress at the wall becomes;

$$\tau_{xy} = K\left|\frac{\partial u}{\partial y}\right|^{n-1}\frac{\partial u}{\partial y}$$

$$\tau_w = K\left(\frac{\partial u}{\partial y}\right)^n \quad @\ y=0$$

$$= K\left[\frac{Re}{(n+1)\,\xi}\right]^{\frac{n}{n+1}}\left(\frac{U_e}{U_\infty}\right)^n\left(\frac{r}{L}\right)^n\left(\frac{U_e}{L}\right)^n[f''(0)]^n \tag{4.1}$$

Since the local friction coefficient can be defined as $C_f = \tau_w/(1/2\rho U_\infty^2)$, then

$$C_f = \frac{2K\left[\frac{Re}{(n+1)\,\xi}\right]^{\frac{n}{n+1}}\left(\frac{U_e}{U_\infty}\right)^n\left(\frac{r}{L}\right)^n\left(\frac{U_e}{L}\right)^n[f''(0)]^n}{\rho U_\infty^2}$$

$$= 2\left[\frac{1}{(n+1)\,\xi}\right]^{\frac{n}{n+1}}Re^{\frac{-1}{n+1}}\left(\frac{U_e}{U_\infty}\right)^{2n}\left(\frac{r}{L}\right)^n[f''(0)]^n \tag{4.2}$$

Rearranging terms into a form that is similar to what is used with Newtonian fluids creates

$$\frac{1}{2}C_f Re^{\frac{1}{n+1}} = \left[\frac{1}{(n+1)\xi}\right]^{\frac{n}{n+1}}\left(\frac{U_e}{U_\infty}\right)^{2n}\left(\frac{r}{L}\right)^n[f''(0)]^n \tag{4.3}$$

Equation (4.3) can be evaluated for the spherical body studied and the value of $1/2C_f Re^{1/(n+1)}$ determined. The results of this evaluation for n=0.600, 1.000, and 1.400 are shown versus x/R in Figure 4.1. The friction coefficient increases with increasing values of the rotation parameter W. It also increases with an increasing x/R to a maximum between x/R=0.95 and 1.00, and then begins to decrease.

The accuracy of this study is reflected in the comparison the results for the Newtonian fluid portion of this analysis with the results for the first term from Lee et al. [8]. As shown in Table 4.1, the present results are almost identical to Lee's first term solutions.

Table 4.1 Comparison of $1/2C_f Re^{1/(n+1)}$ for a rotating sphere in Newtonian flow.

		W = 1.5		W = 3.0		W = 4.7434	
Λ	x/R	Present	Lee	Present	Lee	Present	Lee
0.40	0.951	1.8271	1.8272	2.6217	2.6217	4.0254	4.0255
0.30	1.215	1.6797	1.6797	2.3520	2.3521	3.5466	3.5466
0.20	1.374	1.3941	1.3941	1.8755	1.8754	2.7393	2.7392
0.10	1.486	1.0814	1.0814	1.3459	1.3460	1.8313	1.8314

The values of W (1.0 and 3.16228) used in the development of Figure 4.1 correspond with the values of "BP" (1.0 and 10.0 respectively) used by Kleinstreuer and Wang [11]. Comparing points from Figure 4.1 for n=0.6 with equivalent values of x/R in Kleinstreuer and Wang show good correlation for the forward portion of the boundary layer. As x/R increases the discrepancy between the analyses increases, where at x/R=1.5 the difference is about 10%. This difference can be attributed to this analysis including only the first term of the series. If additional terms were included it is anticipated the results would not vary.

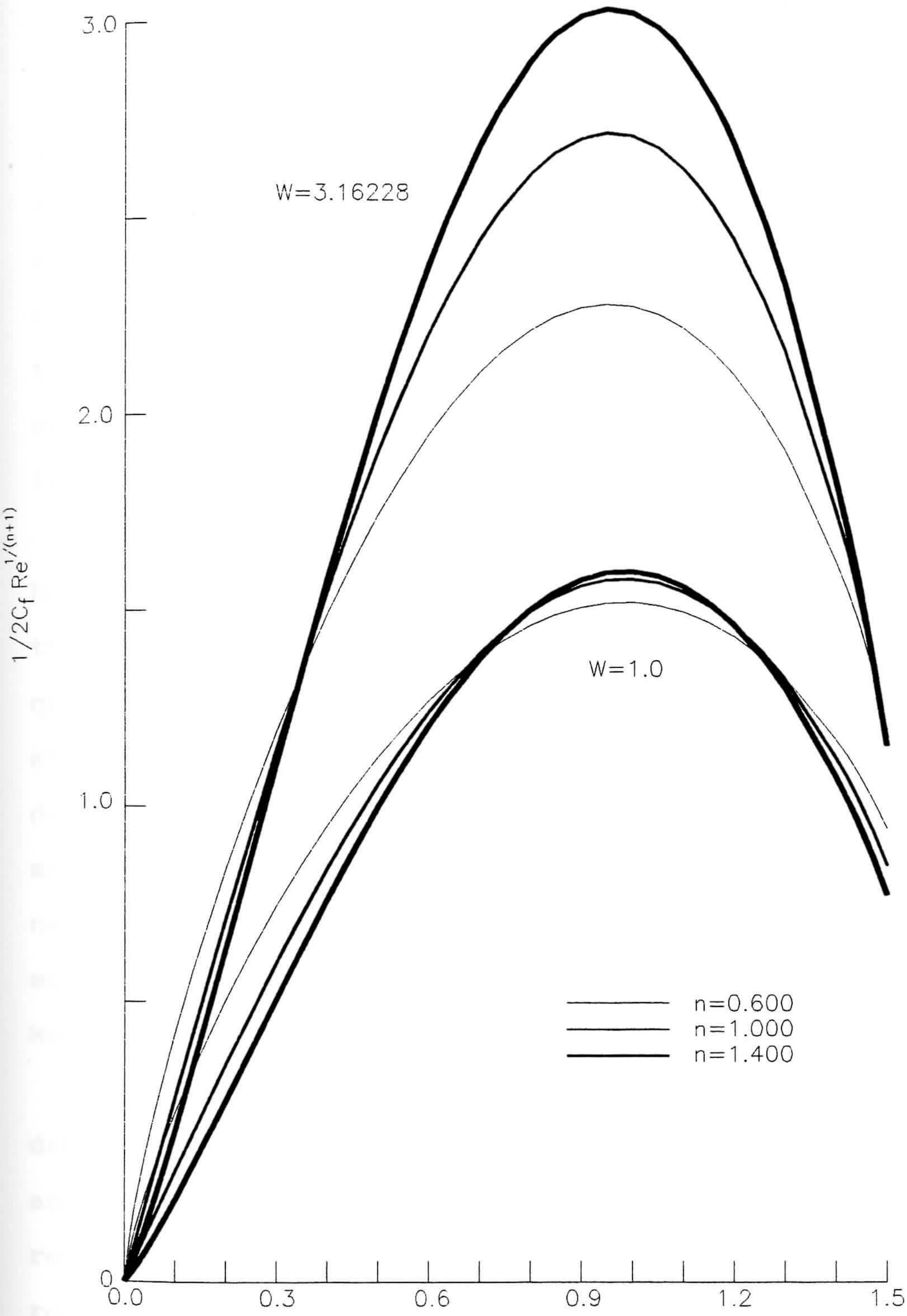

Fig. 4.1 Friction coefficient in terms of $1/2C_f Re^{1/(n+1)}$ for n=0.600, 1.000, and 1.400, for W=1.0 and 3.16228

Chapter V. Conclusion

The problem of analyzing external laminar boundary-layer flow over axisymmetrical bodies in power-law flow was successfully resolved using the Merk-Meksyn technique. Several studies have shown the Merk-Meksyn method as one of the most accurate analytical tools for Newtonian flows over rotating axisymmetrical bodies. Here the analysis was successfully extended into the analysis of Non-Newtonian power-law fluid flow.

A typical Merk-Meksyn method solution for non-rotating bodies leads to solutions of the differential equations in the form of universal functions. The solution sets of sequential ordinary differential equations presented in this study contain general geometric parameters that must be determined for the particular two dimensional or axisymmetrical body in question. While being additional work necessary for the solution, the determination of the parameters does not present itself as a detriment to using the Merk-Meksyn method.

Velocity gradients for the first term of the series determined from the solution of the equations for rotating and non-rotating spheres were respectively compared to results for rotating spheres in Newtonian flow and non-rotating spheres in power-law flow. In both instances the correlation was excellent with results agreeing out to six significant digits.

Further use of this data to calculate the wall shear stress was fairly successful, with a slight discrepancy present from the previously published results. This difference of results appeared only when comparing the present solution to solutions involving more than the initial term in the series. It can therefore be proposed that further work be planned to include additional terms which would decrease the apparent differences between the solutions.

BIBLIOGRAPHY

1. Skelland, A. H. Non-Newtonian Flow and Heat Transfer. Wiley, 1965.

2. Acrivos, A. M., M. J. Shaw, and E. E. Petersen. "Momentum and Heat Transfer in Laminar Boundary-Layer Flows of Non-Newtonian Fluids Past External Surfaces." A.I.Ch.E. Journal. Vol. 6. No. 2. (1960): 312-17.

3. Lee, S. Y., and W. F. Ames. "Similarity Solutions For Non-Newtonian Fluids." A.I.Ch.E. Journal. Vol. 12. No. 4. (1966): 700-08.

4. Merk, H. J. "Rapid Calculations For Boundary-Layer Transfer Using Wedge Solutions and Asymptotic Expansions." Journal of Fluid Mechanics. 5 (1959): 460-80.

5. Chao, B. T., and R. O. Fagbenle. "On Merk's Method of Calculating Boundary Layer Transfer." Int. J. of Heat Mass Transfer. Vol. 17. (1974): 223-40.

6. Kim, H. W., and D. R. Jeng. "Convective Heat Transfer in a Laminar Boundary Layer Near the Separation Point." ASME HTD. Vol. 96. (1988): 471-76.

7. Jeng, D. R., K. J. DeWitt, and M. H. Lee. "Forced Convection Over Rotating Bodies With Non-Uniform Surface Temperature." Int. J. of Heat Mass Transfer. Vol. 22. (1979): 89-98.

8. Lee, M. H., D. R. Jeng, and K. J. DeWitt. "Laminar Boundary Layer Transfer Over Rotating Bodies in Forced Flow." Journal of Heat Transfer. Vol. 100. No. 3. (1978): 496-502.

9. Kim, H. W. "Boundary Layer Transfer For Non-Newtonian Power-Law Fluids Over Two Dimensional or Axisymmetrical Bodies." Ph.D. diss., University of Toledo, 1980.

10. Kim, H. W., D. R. Jeng, and K. J. DeWitt. "Momentum and Heat Transfer in Power-Law Fluid Flow Over Two Dimensional or Axisymmetrical Bodies." _Int. J. of Heat Mass Transfer_. Vol. 26. No. 2. (1983): 245-59.

11. Kleinstreuer, C., and T. V. Wang. "Mixed Thermal Convection of Power-Law Fluids Past Standard Bodies With Suction/Injection and Axisymmetric Body Rotation." _Proceedings of the Twenty-Fifth Heat Transfer Conference held in Houston, Texas 1988. ASME HTD_. Vol. 96. Part 2. 27-32.

APPENDIX

```
C
C  THIS PROGRAM IS TO OBTAIN NON-NEWTONIAN FLOW PAST A ROTATING BODY
C
C     MAIN PROGRAM
C     F-ZERO FUNCTION
C
      REAL*8 ETAEND(5),TEST(5),F(15),DF(15),H,ETA,X,Y,LAMDA,NN,ROPTAL,
     1DELPR,ETEST,DELX,DELY,CHKNEG,SAVEH,SDELPR,SAVETA,DNUMX,DNUMY,
     1PRINT,DENOM,A11,A12,A21,A22,B1,B2,E,W,B0,C0,DI0,CHK1,CHK2
      INTEGER*2 IHO1,IM1,IS1,IHU1,IHO2,IM2,IS2,IHU2,IHOE,IME,ISE,IHUE,
     1IYEAR,IMONTH,IDAY,IC
C
C  A SUBROUTINE TO DESCRIBE DIFFERENTIAL EQUATIONS
      EXTERNAL DIFF
C
      COMMON NN,LAMDA,ROPTAL,W,B0,C0,DI0,INDEX,CHKNEG,CHK1,CHK2
      IC=0
      CHK1=0.D0
      CHK2=0.D0
C
C  INPUT DATA, AND DEFINE OUTPUT FILE
C
      OPEN(5,FILE='INPUT.DAT')
   25 READ(5,101) NN,H,DELPR,ETEST,ROPTAL
      IF(NN.LT.0.0D0) STOP
      READ(5,100) W,B0,C0
      DI0=2.0D0/3.0D0
      SAVEH=H
      SDELPR=DELPR
      READ(5,102) N,(ETAEND(I),TEST(I),I=1,N)
    1 READ(5,103) LAMDA,SAVETA,X,Y
      IF(LAMDA.LT.-2.0D0) GOTO 25
      IC=IC+1
      IF(IC.EQ.1) OPEN(6,FILE='DATA1.OUT',STATUS='NEW')
      IF(IC.EQ.2) OPEN(6,FILE='DATA2.OUT',STATUS='NEW')
      IF(IC.EQ.3) OPEN(6,FILE='DATA3.OUT',STATUS='NEW')
      IF(IC.EQ.4) OPEN(6,FILE='DATA4.OUT',STATUS='NEW')
      IF(IC.EQ.5) OPEN(6,FILE='DATA5.OUT',STATUS='NEW')
      IF(IC.EQ.6) OPEN(6,FILE='DATA6.OUT',STATUS='NEW')
      IF(IC.EQ.7) OPEN(6,FILE='DATA7.OUT',STATUS='NEW')
```

```
      IF(IC.EQ.8) STOP
      CALL GETTIM(IHO1,IM1,IS1,IHU1)
      CALL GETDAT(IYEAR,IMONTH,IDAY)
      WRITE(6,'(1X,3I4)')IYEAR,IMONTH,IDAY
      WRITE(6,'(1X,3I4)')IHO1,IM1,IS1
      I=1
    2 PRINT=SDELPR
      H=SAVEH
      DELPR=SDELPR
      CHKNEG=0.0D0
      K=0
      WRITE(6,200) NN,LAMDA,H,SAVETA,X,Y
      WRITE(6,205) W,B0,C0
      WRITE(6,201) ETAEND(I),TEST(I),ETEST
C
C    INITIALIZE VARIABLES
C
      INDEX=0
      ETA=0.0D0
      F(1)=0.0D0
      F(2)=0.0D0
      F(3)=X
      F(4)=1.0D0
      F(5)=Y
      F(6)=0.0D0
      F(7)=0.0D0
      F(8)=1.0D0
      F(9)=0.0D0
      F(10)=0.0D0
      F(11)=0.0D0
      F(12)=0.0D0
      F(13)=0.0D0
      F(14)=0.0D0
      F(15)=1.0D0
C
C    DEVELOPING BOUNDARY LAYER UTILIZING THE RUNGE-KUTTA METHOD
C
      CALL RUNGE(15,H,ETA,0,F,DF,SF,SDF,DIFF)
      WRITE(6,202) ETA,(F(J),J=1,5)
      K=K+1
    3 CALL RUNGE(15,H,ETA,1,F,DF,SF,SDF,DIFF)
```

```
      IF(CHKNEG.LT.0.0D0) GOTO 11
      K=K+1
      IF(NN-1.0D0) 4,7,6
    4 IF(DABS(SAVETA-ETA).GT.0.1D0*H) GOTO 5
      PRINT=SAVETA
      H=1.0D1*SAVEH
      DELPR=1.0D1*SDELPR
      GOTO 7
    5 IF(DABS(1.0D1*SAVETA-ETA).GT.0.1D0*H) GOTO 7
      PRINT=1.D1*SAVETA
      H=1.0D2*SAVEH
      DELPR=1.0D2*SDELPR
      GOTO 7
    6 IF(DABS(SAVETA-ETA).GT.0.1D0*H) GOTO 7
      PRINT=SAVETA
      H=1.0D-2*SAVEH
      DELPR=0.1D0*SDELPR
    7 IF(1.0D1*H-(ETAEND(N)-ETA)) 8,9,9
    8 IF((PRINT-ETA).GT.0.1D0*H) GOTO 10
      PRINT=PRINT+DELPR
    9 WRITE(6,203) ETA,F(1),F(2),F(3),F(4),F(5)
   10 IF(ETA.LT.ETAEND(I)) GOTO 3
C
C  CORRECTION PROCEDURE USING NEWTON-RAPHSON AND LEAST-SQUARE TECHNIQUES
C
   11 A11=F(7)*F(7)+F(9)*F(9)+F(8)*F(8)+F(10)*F(10)
      A12=F(7)*F(12)+F(9)*F(14)+F(8)*F(13)+F(10)*F(15)
      A21=A12
      A22=F(12)*F(12)+F(14)*F(14)+F(13)*F(13)+F(15)*F(15)
      B1=-(F(7)*(F(2)-1.0D0)+F(9)*F(4)+F(8)*F(3)+F(10)*F(5))
      B2=-(F(12)*(F(2)-1.0D0)+F(14)*F(4)+F(13)*F(3)+F(15)*F(5))
      DNUMX=B1*A22-B2*A12
      DNUMY=B2*A11-B1*A21
      DENOM=A11*A22-A21*A12
      DELX=DNUMX/DENOM
      DELY=DNUMY/DENOM
      IF(W.EQ.0.0D0) DELY=0.0D0
C
C  X AND Y ARE CORRECTED - INITIAL BOUNDARY CONDITIONS
C
      X=X+DELX
```

```
      Y=Y+DELY
C
C  E IS THE ERROR AT THE OUTER BOUNDARY LAYER EDGE
C
      IF(W) 13,12,13
   12 E=(1.0D0-F(2))*(1.0D0-F(2))+F(3)*F(3)
      IF(DABS(DELX/X).GT.TEST(I)) GOTO 2
      GOTO 14
   13 E=(1.0D0-F(2))*(1.0D0-F(2))+F(3)*F(3)+F(4)*F(4)+F(5)*F(5)
      IF(DABS(DELX/X).GT.TEST(I).OR.DABS(DELY/Y).GT.TEST(I)) GOTO 2
   14 IF(E.LT.ETEST) GOTO 16
   15 IF(I.EQ.N) STOP
      I=I+1
      GOTO 2
   16 WRITE(6,204) ETA,F(1),F(2),F(3),F(4),F(5),K
      CALL GETTIM(IHO2,IM2,IS2,IHU2)
      IHUE=IHU2-IHU1
      ISE=IS2-IS1
      IME=IM2-IM1
      IHOE=IHO2-IHO1
      IF(IHUE) 17,18,18
   17 IHUE=IHUE+100
      ISE=ISE-1
   18 IF(ISE) 19,20,20
   19 ISE=ISE+60
      IME=IME-1
   20 IF(IME) 21,22,22
   21 IME=IME+60
      IHOE=IHOE-1
   22 IF(IHOE) 23,24,24
   23 IHOE=IHOE+24
   24 WRITE(6,211)IHO1,IM1,IS1,IHU1
      WRITE(6,212)IHO2,IM2,IS2,IHU2
      WRITE(6,213)IHOE,IME,ISE,IHUE
      GOTO 1
  100 FORMAT(3D10.3)
  101 FORMAT(5D12.3)
  102 FORMAT(I2/(2D12.3))
  103 FORMAT(2D12.5,2D24.16)
  200 FORMAT(////1X,'NN=',D13.6,3X,'LAMDA=',D13.6,3X,'H=',D13.6,3X,
     1'SAVETA=',D13.6,3X,'X=',D13.6,3X,'Y=',D13.6/)
```

```
  201 FORMAT(/1X,'ETAEND=',D13.6,5X,'TEST=',D13.6,5X,'ETEST=',D13.6/)
  202 FORMAT(//5X,'ETA',17X,'F(1)',16X,'F(2)',16X,'F(3)',16X,'F(4)'
     1,16X,'F(5)',//D13.6,2X,5D20.10)
  203 FORMAT(D13.6,2X,5D20.10)
  204 FORMAT(/D13.6,3X,5D20.10//10X,'NUMBER OF TOTAL STEPS= ',I5//)
  205 FORMAT(/1X,'W=',D13.6,5X,'B0=',D13.6,5X,'C0=',D13.6/)
  206 FORMAT(////1X,'NN=',D13.6,3X,'LAMDA=',D13.6,3X,'H=',D13.6/)
  207 FORMAT(/1X,'SAVETA=',D13.6,3X,'X=',D13.6,3X,'Y=',D13.6/)
  208 FORMAT(//4X,'ETA',11X,'F(1)',9X,'F(2)',9X,'F(3)',9X,'F(4)'
     1,9X,'F(5)',//D10.4,2X,5D13.6)
  209 FORMAT(D10.4,2X,5D13.6)
  210 FORMAT(/D10.4,2X,5D13.6//10X,'NUMBER OF TOTAL STEPS= ',I5//)
  211 FORMAT(1X,'  START TIME:',4I4)
  212 FORMAT(1X,' FINISH TIME:',4I4/)
  213 FORMAT(1X,'ELAPSED TIME:',4I4)
      END
C
      SUBROUTINE DIFF(ETA,H,F,DF)
C
C  THIS SUBROUTINE DEFINES THE DIFFERENTIAL EQUATIONS
C
      REAL*8 F(15),DF(15),ETA,H,LAMDA,NN,W,SQRF,SQRG,B0,C0,DI0,DF8NUM
     1,DF8DEN,DF10NM,DF10DE,DF13NM,DF15NM,ROPTAL
      COMMON NN,LAMDA,ROPTAL,W,B0,C0,DI0,INDEX,CHKNEG,CHK1,CHK2
      DF(1)=F(2)
      DF(2)=F(3)
      IF(INDEX.EQ.1) GOTO 10
      DF(3)=-F(1)*F(3)*DABS(F(3))**(1.0D0-NN)-LAMDA*DABS(F(3))**(1.0D0-
     1NN)*(1.0D0-F(2)*F(2)+B0*W*W*F(4)*F(4))
      IF(NN.LE.1.D0) GOTO 20
      IF(F(3).GT.ROPTAL.OR.DABS(1.0D0-F(2)).GT.ROPTAL) GOTO 20
      INDEX=1
   10 SQRF=DSQRT(F(1)*F(1)*DABS(F(3))**(4.D0-2.0D0*NN)-4.0D0*DABS(F(3))
     1**(2.0D0-NN)*(NN-1.0D0)*(F(2)*F(3)-2.0D0*LAMDA*(F(2)*F(3)-B0*W*W*
     1F(4)*F(5))))
      DF(3)=-0.5D0/(NN-1.0D0)*(F(1)*DABS(F(3))**(2.0D0-NN)+SQRF)
      DF(4)=F(5)
      IF(W) 12,11,12
   11 DF(5)=0.0D0
      GOTO 13
   12 SQRG=DSQRT((W*DI0)**(2.0D0-2.0D0*NN)*DABS(F(5))**(4.0D0-2.0D0*NN)
```

```
     1*F(1)*F(1)-4.0D0*(W*DI0)**(1.0D0-NN)*DABS(F(5))**(2.0D0-NN)*(NN-
     11.0D0)*(F(2)*F(5)-C0*LAMDA*(F(3)*F(4)+F(2)*F(5))))
      DF(5)=-0.5D0/(NN-1.0D0)*((W*DI0)**(1.0D0-NN)*DABS(F(5))**(2.0D0-NN
     1)*F(1)+SQRG)
   13 DF(6)=F(7)
      DF(7)=F(8)
      DF8NUM=-F(6)*DABS(F(3))**(2.0D0-NN)*DF(3)+(NN-2.0D0)*DABS(F(3))
     1**(1.0D0-NN)*F(8)*DF(3)*F(1)+(NN-2.0D0)*DABS(F(3))**(1.0D0-NN)*F(8
     1)*((1.0D0-2.0D0*LAMDA)*F(2)*F(3)-B0*W*W*F(4)*F(5))-DABS(F(3))**
     1(2.0D0-NN)*((1.0D0-2.0D0*LAMDA)*(F(7)*F(3)+F(2)*F(8))-B0*W*W*(F(9)
     1*F(5)+F(4)*F(10)))
      DF8DEN=2.D0*(NN-1.0D0)*DF(3)+F(1)*DABS(F(3))**(2.0D0-NN)
      DF(8)=DF8NUM/DF8DEN
      DF(9)=F(10)
      IF(W) 15,14,15
   14 DF(10)=0.0D0
      GOTO 16
   15 DF10NM=-(W*DI0)**(1.0D0-NN)*((2.0D0-NN)*DABS(F(5))**(1.0D0-NN)*(-F
     1(10))*(F(1)*DF(5)+F(2)*F(5)-C0*LAMDA*(F(3)*F(4)+F(2)*F(5)))+DABS(F
     1(5))**(2.0D0-NN)*(F(6)*DF(5)+F(7)*F(5)+F(2)*F(10)-C0*LAMDA*(F(8)*F
     1(4)+F(3)*F(9)+F(7)*F(5)+F(2)*F(10))))
      DF10DE=2.D0*(NN-1.0D0)*DF(5)+(W*DI0)**(1.0D0-NN)*DABS(F(5))**(2.0D
     10-NN)*F(1)
      DF(10)=DF10NM/DF10DE
   16 DF(11)=F(12)
      DF(12)=F(13)
      DF13NM=-F(11)*DABS(F(3))**(2.0D0-NN)*DF(3)+(NN-20.D0)*DABS(F(3))
     1**(1.0D0-NN)*DF(3)*F(13)*F(1)+(NN-2.0D0)*DABS(F(3))**(1.0D0-NN)*
     1F(13)*((1.0D0-2.0D0*LAMDA)*F(2)*F(3)-B0*W*W*F(4)*F(5))-DABS(F(3))
     1**(2.0D0-NN)*((1.0D0-2.0D0*LAMDA)*(F(12)*F(3)+F(2)*F(13))-B0*W*W*
     1(F(14)*F(5)-F(4)*F(15)))
      DF(13)=DF13NM/DF8DEN
      DF(14)=F(15)
      IF(W) 18,17,18
   17 DF(15)=0.0D0
      GOTO 19
   18 DF15NM=-(W*DI0)**(1.0D0-NN)*((2.0D0-NN)*DABS(F(5))**(1.0D0-NN)*
     1(-F(15))*(F(1)*DF(5)+F(2)*F(5)-C0*LAMDA*(F(3)*F(4)+F(2)*F(5)))+
     1DABS(F(5))**(2.0D0-NN)*(F(11)*DF(5)+F(12)*F(5)+F(2)*F(15)-C0*LAMDA
     1*(F(13)*F(4)+F(3)*F(14)+F(12)*F(5)+F(2)*F(15))))
      DF(15)=DF15NM/DF10DE
```

```
   19 RETURN
   20 DF(4)=F(5)
      IF(W) 22,21,22
   21 DF(5)=0.0D0
      GOTO 23
   22 DF(5)=-(W*DIO)**(1.0D0-NN)*DABS(F(5))**(1.0D0-NN)*(F(1)*F(5)-
     1C0*LAMDA*F(2)*F(4))
   23 DF(6)=F(7)
      DF(7)=F(8)
      DF(8)=-DABS(F(3))**(1.0D0-NN)*(F(6)*F(3)+F(1)*F(8)-2.0D0*LAMDA*(
     1F(2)*F(7)-B0*W*W*F(4)*F(9)))-(1.0D0-NN)*DABS(F(3))**(-NN)*F(8)*(
     1F(1)*F(3)+LAMDA*(1.0D0-F(2)*F(2)+B0*W*W*F(4)*F(4)))
      DF(9)=F(10)
      IF(W) 25,24,25
   24 DF(10)=0.0D0
      GOTO 26
   25 DF(10)=(W*DIO)**(1.0D0-NN)*((1.0D0-NN)*DABS(F(5))**(-NN)*(-F(10))*
     1(C0*LAMDA*F(2)*F(4)-F(1)*F(5))+DABS(F(5))**(1.0D0-NN)*(C0*LAMDA*
     1(F(7)*F(4)+F(2)*F(9))-F(6)*F(5)-F(1)*F(10)))
   26 DF(11)=F(12)
      DF(12)=F(13)
      DF(13)=-DABS(F(3))**(1.0D0-NN)*(F(11)*F(3)+F(1)*F(13)-2.0D0*LAMDA*
     1(F(2)*F(12)-B0*W*W*F(4)*F(14)))-(1.0D0-NN)*DABS(F(3))**(-NN)*F(13)
     1*(F(1)*F(3)+LAMDA*(1.0D0-F(2)*F(2)+B0*W*W*F(4)*F(4)))
      DF(14)=F(15)
      IF(W) 28,27,28
   27 DF(15)=0.0D0
      GOTO 29
   28 DF(15)=(W*DIO)**(1.0D0-NN)*((1.0D0-NN)*DABS(F(5))**(-NN)*(-F(15))*
     1(C0*LAMDA*F(2)*F(4)-F(1)*F(5))+DABS(F(5))**(1.0D0-NN)*(C0*LAMDA*
     1(F(12)*F(4)+F(2)*F(14))-F(11)*F(5)-F(1)*F(15)))
   29 RETURN
      END
C
      SUBROUTINE RUNGE(N,H,X,ISET,F,DF,SF,SDF,DIFF)
C
C   THIS SUBROUTINE DEFINES THE RUNGE-KUTTA PROCEDURE
C
      REAL*8 F(15),DF(15),P(15),FR(15),C2(15),C3(15),C4(15),DFR(15)
     1,H,X,LAMDA,NN,CHKNEG,ROPTAL,W,B0,C0,DIO,CHK1,CHK2,SF(15),SDF(15)
      COMMON NN,LAMDA,ROPTAL,W,B0,C0,DIO,INDEX,CHKNEG,CHK1,CHK2
```

```
      IF(ISET.GT.0) GOTO 10
      CALL DIFF(X,H,F,DF)
      RETURN
   10 DO 1001 I=1,N
      SF(I)=F(I)
      SDF(I)=DF(I)
 1001 P(I)=F(I)+H/2.D0*DF(I)
      IF(P(3).LT.0.D0) GOTO 30
      IF(P(5).GT.0.D0) GOTO 50
      CALL DIFF(X+H/2.D0,H,P,C2)
      DO 1002 I=1,N
 1002 P(I)=F(I)+H/2.D0*C2(I)
      IF(P(3).LT.0.D0) GOTO 30
      IF(P(5).GT.0.D0) GOTO 50
      CALL DIFF(X+H/2.0D0,H,P,C3)
      DO 1003 I=1,N
 1003 P(I)=F(I)+H*C3(I)
      IF(P(3).LT.0.D0) GOTO 30
      IF(P(5).GT.0.D0) GOTO 50
      CALL DIFF(X+H,H,P,C4)
      DO 1004 I=1,N
 1004 FR(I)=F(I)+H/6.D0*(DF(I)+2.D0*C2(I)+2.D0*C3(I)+C4(I))
      IF(FR(3).LT.0.D0) GOTO 40
      IF(FR(5).GT.0.D0) GOTO 60
      CALL DIFF(X+H,H,FR,DFR)
   20 X=X+H
      DO 1201 I=1,N
      F(I)=FR(I)
 1201 DF(I)=DFR(I)
      RETURN
   30 CHKNEG=P(3)
      RETURN
   40 CHKNEG=FR(3)
      RETURN
   50 CHKNEG=-P(5)
      RETURN
   60 CHKNEG=-FR(5)
      RETURN
      END
```